The Versatility of Polymers in Perovskite Solar Cells

Abolfazl Ghaderian[1], Roghayeh Heiran[2], Samrana Kazim[1,3], Shahzada Ahmad[1,3]

[1] BCMaterials, Basque Center for Materials, Applications, and Nanostructures, Bld. Martina Casiano, UPV/EHU Science Park, Barrio Sarriena s/n, 48940 Leioa, Spain
[2] Department of Chemistry, Estahban Higher Education Center, 74519 44655, Estahban, Iran
[3] IKERBASQUE, Basque Foundation for Science, Bilbao 48009, Spain
E-mail address: shahzada.ahmad@bcmaterials.net

Abstract

The development of sustainable, cost-effective, and un-depleted energy resources is a demanding challenge for researchers and technologists. Harvesting an abundant source of energy such as solar light is one of the promising ways, to convert sunlight radiation through a semiconductor directly into electricity. Varieties of solar cells based on silicon, thin-film, and emerging solar cells are being developed to address these challenges, and some of them reached market maturity. Emerging solar cells also provide the possibility of manufacturing flexible devices with high efficiency, low materials use, and subsequently low module cost. Among them, perovskite solar cells (PSCs) emerged as being efficient with high potential for a commercial endeavor. Nonetheless, there is a window of opportunity that exists to improve lifetime, photovoltaic (PV) performances, and further reduction of cost, before its commercial viability. Employing polymers is one of the promising strategies to increase the reliability and upgrade the PV performances such as improving fill factor (FF), open-circuit voltage (V_{oc}), short-circuit current density (J_{sc}), and thus power conversion efficiency (PCE). Here we present recent progress in the use of polymeric materials as hole transporting material (HTM) and electron transporting material (ETM), interfacial layer, and additives into the perovskite, to improve stability and photovoltaic properties.

Keywords: Photovoltaics, Perovskite solar cell, Polymer, Synthesis, performance, Stability.

1. Introduction

Solar energy is an environmentally friendly, reliable, and unlimited source of energy that can be converted into electrical energy through the photovoltaic process without any substantial harmful effect on the environment.[1,2] Solar cells can be classified into three categories. The first-generation solar cells are based on crystalline silicon wafers (c-Si), also known as silicon wafer-based technology, and are efficient, and reliable with high power efficiency. They have reached high market maturity and penetration but are heavy, rigid, and with high technology manufacturing costs. It is paramount, to replace silicon photovoltaics (PV) with flexible, lightweight, cost-effective, and easy-to-

fabricate solar cells. The second-generation solar cells termed thin-film solar cells consist of two heterojunction layers between two contact layers. Made by a multilayer thin film with a thickness of 2.5 μm (compared to 170-250 μm for first-generation) on a substrate made of metal, glass, or polymer. The second-generation solar cells show fewer processing steps, and simpler fabrication technology than the first generation and include amorphous silicon (a-Si), copper indium selenide (CIS), copper indium gallium selenide (CIGS), and cadmium telluride (CdTe) solar cells.[3–6] The third-generation solar cells enjoy synergistic benefits of the earlier version and in the last decades, become a topic of significant interest to supply high future energy demand. Organic photovoltaic (OPV), dye-sensitized solar cells (DSSCs), quantum dot sensitized solar cells (QDSSCs), and perovskite solar cells (PSCs) are among the developed third-generation solar cells.[4–7] PSCs are a relative discovery among solar cells, and achieved significant consideration in PV technology during the past decade, owing to their crystalline structure, unique optoelectronic properties, low processing cost, and high power conversion efficiencies (PCEs) which are on par with the well-developed silicon-based solar cells.[8,9] Calcium titanium oxide ($CaTiO_3$), is a type of perovskites, a mineral, named after a Russian mineralogist L.A. Perovski. Perovskites are exceptional candidates for photovoltaic (PV) applications with strong solar absorption, and high optoelectrical properties. The perovskite is typically described by the formula ABX_3, they have a cubic unit cell, A and B are cations of different sizes, and the larger A cation occupies a cubo-octahedral site shared with twelve X anions. Either tin (Sn) or lead (Pb) is the B cation, and X represents an anion (halogens like chlorine, bromine, and Iodine). A is typically an inorganic or organic cation such as methylammonium ($CH_3NH_3^+$), ethyl ammonium ($CH_3CH_2NH_3^+$), or formamidinium ($CH(NH_2)_2^+$). In case A was replaced by an organic cation, organic-inorganic hybrid materials will be created. The nature of A deeply influences the optoelectronic properties and stability of the perovskite layer. The crystal structure of perovskite is illustrated in **Fig.1**.[10–13]

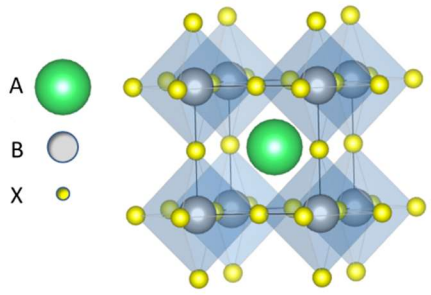

Fig.1. Polyhedral representation of the cubic perovskite structure ABX_3, A: MA or FA cation, B: Pb^{2+} cation, X: Cl-, Br- or I- anion.

The typical structure of PSC devices is composed of i) a layer of perovskite active layer as a light absorption layer, which generates free charge carriers upon photoexcitation, ii) charge transporting materials (CTMs) including HTM and ETM. Perovskite active layer is sandwiched between the hole transporting material (HTM) and electron transporting material (ETM). ETM extracts and transports electrons from the active layer to the cathode and HTM extracts and transports holes to the anode, and iii) electrodes (Au, Ag, Al, or Cu) consist of cathode and anode. Depending on how the charge selective layers are positioned, the PSCs can be divided into regular (conventional), and inverted structures. The position of regular structure (*n-i-p*) is glass substrate/cathode/ ETM/ perovskite/HTM/anode, and the inverted (*p-i-n*) PSC is glass substrate/anode/HTM/perovskite/ETM/cathode. PSCs were developed from liquid DSSCs by Miyasaka's research team, in which $CH_3NH_3PbBr_3$ and $CH_3NH_3PbI_3$ were the first reported perovskite as the light absorber. In their initial research (2006) $CH_3NH_3PbBr_3$ was used as the sensitizer in liquid DSSC with an efficiency of 2.19%. Then, in 2009 to improve efficiency they applied $CH_3NH_3PbI_3$, and $CH_3NH_3PbBr_3$ on TiO_2 as n-type semiconductors to sensitize TiO_2 for visible-light conversion in photovoltaic cells, and the efficiency was improved to 3.80% on a $CH_3NH_3PbI_3$–based cell.[14] PSCs can be classified into two main categories, mesoporous and planar structures (**Fig.2**). The mesoporous structure was the most common device structure in the early stage of the introduction of PSCs. The fabrication of mesoporous devices needs repeated sintering of TiO_2 at high temperatures, while the fabrication of planar structures is relatively simple. The inverted planar (*p-i-n*) PSCs have numerous potential for commercialization as compared with the mesoporous, owing to their multiple advantages such as simple fabrication procedures, moderate processing temperature, less hysteresis effect, high interface stability, and shorter process time.[15–17]

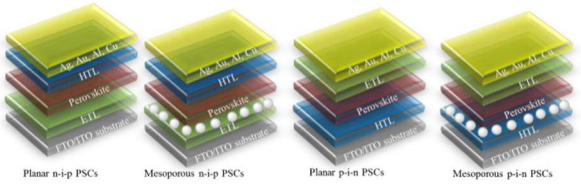

Fig.2. The illustration of a typical perovskite solar cell, the conventional (*n-i-p*) and inverted (*p-i-n*) structures

When perovskite absorbed a photon with energy greater than the perovskite bandgap, the perovskite layer is excited, and generated charge careers (electrons and holes) that

are transported through the ETM and HTM. The separation of charge carriers inside the materials and interface formed conduction band electrons and valence band holes. Electrons and holes are injected into the conduction band of ETM and valence band (HOMO) of inorganic (organic) HTM, and the collection of charge carriers at the respective electrodes takes place to complete the circuit (**Fig.3**).[18]

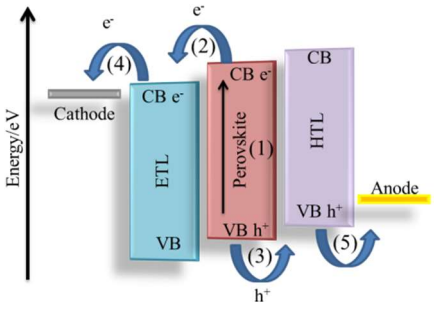

Fig.3. Schematic representation of energy levels and charge transfer processes in PSCs.

Since the pioneering work in 2009, sincere efforts have been made to enhance the PV performance of PSCs, and very recently, Chen *et al.* introduced monolithic perovskite/organic tandem solar cells with 23.60% (22.95% certified) efficiency.[19] Although different research groups have focused on this issue, the PSCs still display poor stability as compared to silicon solar cells. Various strategies have been employed to tackle this problem including designing new perovskites with high stability, introducing novel HTM or ETM, and interfacial engineering by modifying absorber layer, HTM, or ETM. Last year's polymer integration has emerged as a promising pathway to produce PSCs with a high lifetime. Polymer strategy not only enhances device stability but also improves device performance since the polymer material has an extended π-conjugated system which can harness sunlight more efficiently and can generate a circuit by charge transport. Also, there is a possibility of mixing polymers and creating a blend to absorb light in a wide spectrum. Moreover, polymers have shown high-quality film-forming properties together with the potential of preparing flexible solar cells which can in principle offer production in high volume at low process cost.

Conjugated polymers have excellent charge transfer properties with superior stability and are promising materials to be used as HTM. A PCE of 22.30% with remarkable device stability has been shown by utilizing a pyrene-based polymer termed PE10 as HTM.[20] Moreover, perylene diimide (PDI), naphthalene diimide (NDI), and polyfluorenes based polymeric ETM have been introduced into PSCs.[21] Fang *et al.* introduced a PDI-based polymer, PFPDI, as ETM. The device fabricated with PFPDI exhibited J_{sc} of 23.43 mA

cm^{-2} with an overall PCE of 15.01% which was comparable to the PCBM-based device.[22]

Polymers with various functional groups have been used as additives in the perovskite to enhance the interaction between the grains in the perovskite layer, and also increase the perovskite thin-film quality, which leads to improved device stability and performance.[23] Grätzel *et al.* used poly (methyl methacrylate) (PMMA) as a template to regulate the nucleation and crystal growth of perovskite film.[24] The incorporation of the polymeric passivation layer between the perovskite layer and adjacent transport layers protects the active layer from moisture or environmental attack. Boo *et al.* reported a PCE of 15.10% by using polyaniline (PANI) as an interfacial layer between the perovskite layer and ETM.[25] However, PANI is known to convert from one phase to another at room temperature.

In this communication, we reviewed the role of polymers as HTM, ETM, as an interfacial layer, and additives in the perovskites absorber, as well as polymers to improve stability and photovoltaic properties.

2. Polymers as HTM

Hole transporting materials (HTMs) play an essential role in PSCs, they can extract and transport holes from the perovskite to the metal electrode. Moreover, they improve the stability of the devices and minimize the charge recombination and the energy barrier between perovskite and electrode.[9] Polymeric HTMs have attracted considerable attention owing to their mechanical flexibility, film-forming properties, thermal stability, and less corrosive effects on electrodes.[26] The structure and summary of some polymeric HTMs are presented in **Scheme 1** and **Table 1**, respectively.

Poly-[bis(4-phenyl)(2,4,6-trimethylphenyl)amine] (PTAA), as a promising candidate was the first polymer studied as HTM in PSCs and achieved high efficiency. The nanocomposite of mesoporous TiO_2/$CH_3NH_3PbI_3$/PTTA-based PSC obtained a maximum PCE of 12.00% even higher than that based on 2,2′,7,7′-tetrakis-(N,N-di-p-methoxyphenylamine)9,9′-spirobifluorene (spiro-OMeTAD) (8.40%) under standard AM 1.5 conditions.[27] Later, the device fabricated by formamidinium lead iodide ($FAPbI_3$) as a perovskite layer exhibited better performance than $CH_3NH_3PbI_3$ because of its broad absorption of the light with a smaller band gap, and a PCE >20.00% was achieved.[28] Moreover, a methoxy-functionalized triarylamine-based polymeric HTM (CH_3O-PTAA) into PSCs with a *n-i-p* structure (fluorine-doped tin oxide (FTO)/blocking layer (bl)-TiO_2/mesoporous (mp)-

TiO_2/$(FAPbI_3)_{0.85}(MAPbBr_3)_{0.15}$/$CH_3O$-PTAA/Au) enhanced the doping ability, conductance, and stability as compared to the common CH_3-PTAA. PSCs based on doped CH_3O-PTAA exhibited PCEs of up to 21.00% and excellent long-term thermal stability after damp-heat test in the dark storage conditions (ISOS-D-3) of 85 °C and 85% relative humidity (RH) for over 1000 h. The methoxy group at the para(*p*-) position of the PTAA in CH_3O-PTAA enhanced the stability and doping ability due to resonance stabilization effect and favourable interaction of oxygen atom in methoxy group with Li^+ ion. The radical delocalization of triarylamine through resonance improve the stability of the CH_3O-PTAA radical cation, suppressing radical quenching. Higher doping ability and conductance of CH_3O-PTAA are the results of upshifted HOMO energy level, favourable interaction of oxygen atom with Li^+ and resonance stability of CH_3O-PTAA compared with CH_3-PTAA.[29] In another report, methyl-functionalized PTAA was synthesized through the Suzuki polycondensation and used as HTM in dopant-free PSCs with *n-i-p* configuration. The PV properties of the fabricated device (17.60%) PCE enhances as compared to the reference device based on commercial PTAA (PCE of 16.70%).[30]

Although significant works with promising results have been demonstrated based on PTAA, however, PTAA is not a good choice in inverted structures in terms of its low refractive index. Texturing PTAA by simply mixing polystyrene (PS) with PTAA and then washing them away from the PTAA film was an efficient way to reduce reflection, achieving an efficiency improvement from 18.30% to 20.80%. By using an antireflection coating on glass more light can be transmitted into the device, and the efficiency was further improved to 21.60%, which is among the highest efficiencies of the inverted PSCs with low-temperature processing.[31] Very recently, few-layered 2D-black phosphorus (BP) nanosheet doped PTAA has been introduced as HTM for planar *p-i-n* type PSCs. The black phosphorus doping increases the conductivity and hydrophobicity of the PTAA, and this improves the charge extraction efficiency with a reduced energy barrier at the perovskite/black phosphorus:PTAA interface. The high-quality device, led to a high PCE of 20.49% with an open-circuit voltage (V_{oc}) of 1.106 V, a short-circuit current density (J_{sc}) of 22.43 mA/cm^2, and a FF of 82.60%, superior to 18.26% of the control PSC with excellent stability, which can maintain over 80% of its initial efficiency after 800 h storage under 45% relative humidity at room temperature was demonstrated.[32] The certified PCE of single-junction planar inverted PSCs based on PTAA has achieved 22.30% (23.00% power conversion efficiency for lab-measured

champion devices) by PSCs based on CsFAMA films. The *p–i–n* planar heterojunction PSCs were structured as indium tin oxide (ITO) glass substrate/(PTAA)/perovskite/fullerene(C_{60})/bathocuproine (BCP)/copper. Using a trace amount of surface-anchoring alkyl amine ligands (AALs) added to the precursor solution suppresses non-radiative carrier recombination and improves the optoelectronic properties of perovskite films with good operational stability (1,000 h at the maximum power point under simulated AM1.5 illuminations, without loss of efficiency).[33]

Poly(3,4-ethylenedioxythiophene):poly(styrenesulfonate) (PEDOT:PSS) is a widely used polymer HTM in PSCs because of its high optical transparency, easy fabrication process, good mechanical flexibility, as well as suitable energy levels. However, the initial results were not satisfactory and hydrophilicity limits the PCE along with storage stability of PEDOT: PSS-based PSCs.[34] The first inverted PSCs adopted PEDOT:PSS as HTM on the glass/ITO/PEDOT:PSS/ $CH_3NH_3PbI_3/C_{60}$/BCP/Al configuration produced a PCE of 3.90% in 2013.[35] Until now, the inverted PSCs-based PEDOT:PSS HTM has achieved a PCE of 18%, by assembling PEDOT:PSS monolayers on the ITO surface through the water rinsing process.[36]

poly(3-hexylthiophene) (P3HT) is thiophene (electron-rich monomer) based polymer with attached $–(CH_2)_5CH_3$ side chains, an alternative HTM, with excellent optoelectronic properties, relatively high hole mobility, good stability, and ease of synthesis,[26] and is among one of the few feasible conjugated polymers for large-scale production to date. The use of P3HT as HTM in PSCs firstly started from PCE of 0.52% using the P3HT/$CH_3NH_3PbBr_3$-coated alumina scaffold in 2013.[37] Despite the potential advantages of P3HT, the resulting cells have a low V_{oc} due to recombination at the perovskite/P3HT interface. Seo *et al.* introduce a double-layered halide (DLH) structure in which an ultrathin wide-bandgap halide was inserted between the perovskite absorber layer and P3HT to reduce interface recombination and improve PCE, and a PCE of 23.30% achieved for the best-performing device. Moreover, the DLH-based PSCs yielded certified PCEs of 22.70% with a low hysteresis of ±0.51% for small-area and 16.00% for a large-area system, a promising candidate for commercial PSCs.[38]

Without using any additional absorber layer or any interlayer at the perovskite/P3HT (PSK/P3HT) interface, a PCE of 19.25%, 16.29%, and 13.30% for small area (0.1 cm^2), large area (1.0 cm^2), and perovskite solar module (43 cm^2 active area) was achieved, respectively by doping Li-TFSI, t-BP, and FK209 Co(III)-TFSI into triple-cation/double-halide hybrid perovskite ($(FA_{1-x-y}MA_xCs_y)Pb(I_{1-x}Br_x)_3$) mesoscopic

PSCs.[39] On the other hand, the charge transport properties of P3HT can be improved by the addition of a dopant.[39] Jeong *et al.* indicated incorporating gallium(III) acetylacetonate ($Ga(acac)_3$) in P3HT could improve moisture stability and PCE with an efficiency of over 24.00%.[40] Furthermore, the introduction of acceptor monomers into the P3HT chain achieved donor-acceptor (D-A) copolymers to improve device performance.[41,42] Introduction of benzothiadiazole (BTD) as electron-poor moiety into P3HT creates a D-A system that improves the charge mobility through HTM in flexible PSC.[43]

Poly{2,7-[(5,5-bis(3′,7′-dimethyloctyl)-5H-1,8-dithia-as-indacenone]-alt-5,5-[5′,6′-bis(octyloxy)-4′,7′-di-2-thienyl-2′,1′,3′-benzothiadiazole] (PDTIDTBT), a D-A type copolymer, with good mobility, great hole-transporting property, and excellent optical properties used in fabrication of the mesoscopic PSCs as HTM with a PCE of 17.90%. Although this efficiency was lower than Spiro-OMeTAD, the deposition of a thin layer of PMMA at the perovskite/HTM interface pushed to an impressive PCE of 19.89%, which is better than PMMA/Spiro-OMeTAD-based PSC (19.28%). The PDTIDTBT-based PSC exhibited excellent operational stability with only 8% PCE loss after 200 h under continuous illumination.[44]

In addition to PCE, device stability plays a key role in the commercialization of PSCs, and researchers have focused on this issue as well. Two D-A type polymers involving fused dithienopiceno carbazole (DTPS) with the planar conformation, the narrow bandgap of the DTPC unit, and strong electron-donating property were employed as the polymeric dopant-free HTMs by Gao *et al.* PDTPC as a suitable HTM delivered an impressive PCE of 16.96%, with high hole mobility up to 4×10^{-3} cm^2 V^{-1} s^{-1}. The dopant-free PDTPC-based PSCs exhibited excellent stability sustaining 96% of the initial efficiency without encapsulation for 1300 h of storage in ambient air.[45]

Poly(1,4-(2,5-bis((2-butyloctyloxyphenylene)-2,7-(5,5,10,10-tetrakis(4-hexylphenyl)-5,10-dihydro-s-indaceno[2,1-b:6,5-b′] dithiophene)) (IDTB) copolymer, with high moisture stability (remain 80% of initial PCE in 65% RH after 10 days), and low hysteresis (0.44%) was employed as HTM in a planar *n-i-p* based PSCs. The intramolecular S…O interactions (red dash line) between indaceno[2,1-b:6,5-b′] dithiophene (IDT) and 2,5-bis ((2-butyloctyloxyphenylene (B) monomers result a high planar ladder-like conjugated IDTB copolymer. IDTB copolymer effectively passivated the defects in the perovskite layer and exhibited high hole mobility and hole-extracting abilities due to strong interactions of the O and S atoms in the backbone with Pb ions of

the perovskite layer. As a result, IDTB-based PSC showed V_{oc} of 1.107 V, J_{sc} of 23.06 mA cm^{-2}, FF of 75.90%, as well as, PCE of 19.38%, while the spiro-OMeTAD-based reference PSC exhibited V_{oc} of 1.073 V, J_{sc} of 23.78 mA cm^{-2}, FF of 71.40%, and PCE of 18.22%.[9] The higher V_{oc} and FF values of the polymeric modified device are attributed to its deep homo level and its high hole mobility.

Pyridine-based polymer, called PPY2, with passivation function, can suppress the non-radiative recombination processes inside the perovskite and at its interface by the formation of high-quality polycrystalline perovskite films when used as the HTM in inverted PSCs. Upright optical transparency of PPY2 in the visible region makes them a worthy HTM, and dopant-free PPY2 based PSC can reach a remarkable PCE up to 22.41% with a high V_{oc} of 1.16, and excellent long-term photo-stability, as over 97% of its initial PCE retain after one sun constant illumination for 500 h.[46]

To overcome the low conductivity of such polymers, the tactic of using a composite of activated multiwall carbon nanotube (CNT), and Lewis-base polymer as additive was a highly effective method for the fabrication of small area (0.16 cm^2), large-area (1.0 cm^2), and flexible devices. Highly conductive CNTs can facilitate effective hole-extraction and charge transport from perovskite to the HTM, and polymers can act as passivating material. The PSCs based on the PMMA-CNTs exhibited an excellent PCE of 21.70%, 20.70%, and 18.30% for small-, and large-area PSCs, and flexible PSCs, respectively.[47]

3. Polymers as ETM

Electron transport materials (ETMs) play an important role in receiving and transporting electrons. For a competent charge transfer and hole blocking, the ETMs should have aligned energy levels with perovskite, and for the suitable electron-transporting ability to the cathode, the electron mobility of ETM should be high. In addition, ETM should be flat and smooth with high transmittance, good stability, and low-cost fabrication.[17,48] Fullerene and its derivatives are the most commonly used ETMs, high electron mobility and electron injection from perovskite to fullerene make them good candidates. These derivatives are sensitive to moisture and oxygen, and their structures are difficult to be modified, moreover, at high annealing temperatures, they can aggregate.[49] Only a few examples of polymeric ETMs have been reported in the literature. The structure and summary of some polymers as ETM is presented in **Scheme 1** and **Table 1**, respectively. NDI as an electron-deficient core has been widely used in designing polymeric ETMs. It seems poly {{N,N′-bis(2-octyldodecyl)-1,4,5,8-naphthalene diimide-2,6-diyl]-alt-

5,5′-(2,2′-bithiophene)} (N2200 or P(NDI2OD-T2)), poly {{N,N′-bis(alkyl)-1,4,5,8-naphthalene diimide-2,6-diyl]-alt-5,5′-di(thiophene-2-yl)-2,2′-(E)-2-(2-(thiophen-2-yl)vinyl)thiophene]} (PNVT-8), and (PNDI2OD)TT were the first polymeric ETMs in inverted planar PSC gave a competitive PCE of 8.15, 7.47, and 6.47%, respectively [50] which was shown to be competitive with a control device where PCBM was ETM yielded a PCE of 8.51%.

Yip *et al.* developed an amino-functionalized copolymer that included fluorene, NDI, and thiophene spacers (called PFN-2TNDI) to replace [6,6]-phenyl-C61-butyric acid methyl ester ($PC_{61}BM$), the most popular used ETM, in inverted planar PSCs. The backbone of polymeric ETM is composed of fluorine (with good hole blocking property) and NDI with two thiophene spacers (improved polymer packing and charge transfer property). A high PCE of 16.70% was achieved by PFN-2TNDI as ETM while the control PSC showed a lower PCE of 12.90%.[51] Moreover, an NDI-based polymer contains a copolymer of NDI and dicyano-terthiophene as a highly efficient ETM, namely P(NDI2DT-TTCN), not only enhanced photovoltaic performance with PCE of 17.00% with negligible hysteresis but also improved hydrophobicity, mechanical and light-induced stability as compared with PCBM (**Fig. 4**).[52]

Jiang *et al.* developed a conjugated polymer, poly(naphthodiperylenetetraimide-vinylene) (NDP-V), as an efficient ETM in inverted planar PSC with a maximum PCE of 16.54% and low hysteresis. Compared with $PC_{61}BM$, a fullerene-based ETM, NDP-V demonstrated higher electron mobility, and more hydrophobicity yielding higher performance and stability in PSCs.[49]

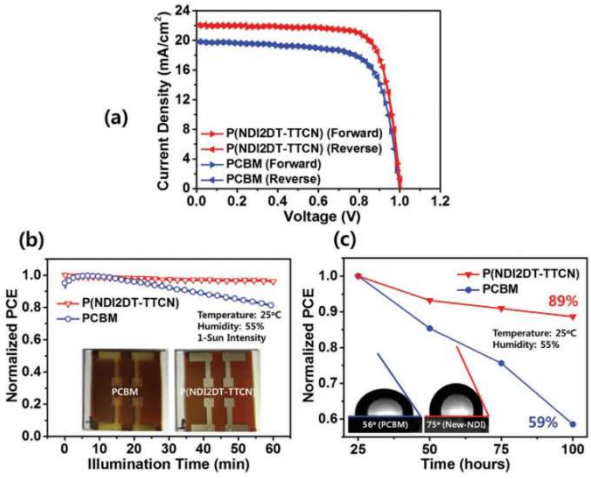

Fig. 4. a) *J–V* characteristic curves, b) light-induced degradation, and c) long-term stability of P(NDI2DT-TTCN) and PCBM-based inverted Pero-SCs, respectively.52 Copyright 201**8**, Wiley-VCH.

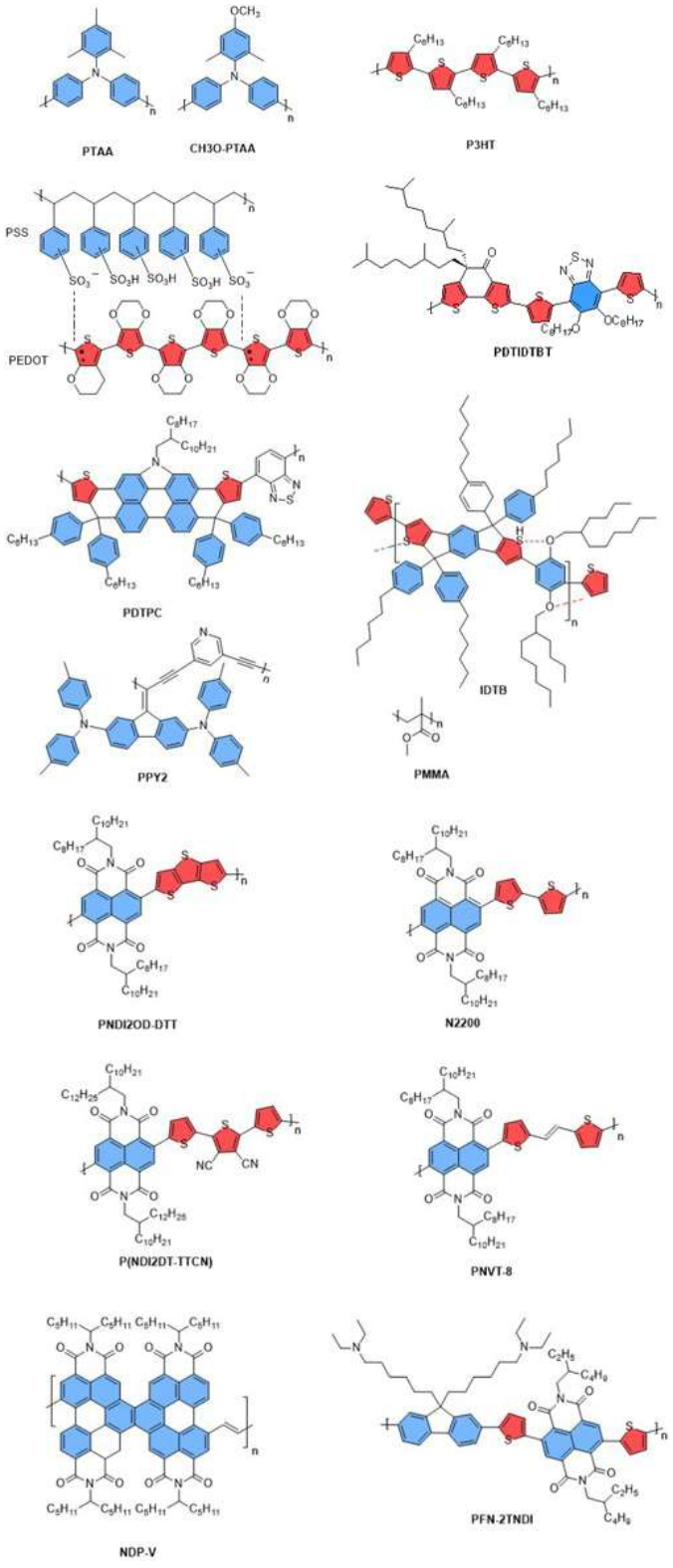

Sche**me 1**. The structure of polymeric charge transport materials. [9,27–45]

Table 1: Photovoltaic performance of PSCs by using some polymeric CTM

Polymer	PCE [%]	J_{sc} [mAcm^{-2}]	V_{oc} [V]	FF [%]	Device structure	Ref.
Poly IDBP (HTM)	19.38	23.06	1.107	75.90	*n-i-p*	[9]
PE10 (HTM)	22.30	24.10	1.160	79.80	*n-i-p*	[20]
PTAA (HTM)	12.00	16.50	0.997	72.70	*n-i-p*	[27]
PTAA (HTM)	20.20	24.70	1.060	77.50	*n-i-p*	[28]
CH_3-PTAA (HTM)	21.16	23.12	1.140	80.30	*n-i-p*	[29]
CH_3O-PTAA (HTM)	>21.00	23.00	1.140	80.40	*n-i-p*	[29]
PTAA (HTM)	17.60	22.10	1.060	75.00	*n-i-p*	[30]
PS/PTAA (HTM)	20.80	22.50	1.120	82.50	*p-i-n*	[31]
BP/PTAA (HTM)	20.49	22.43	1.106	82.60	*p-i-n*	[32]
PTAA (HTM)	22.34	23.90	1.140	82.00	*p-i-n*	[33]
P3HT (HTM)	0.52	1.13	0.840	54.00	*n-i-p*	[37]
P3HT (HTM)	23.30	24.88	1.152	81.40	*n-i-p*	[38]
LiFSI,TBP,Co(III)-TFSI /P3HT (HTM)	19.25	23.86	1.090	73.70	*n-i-p*	[39]
GA/ P3HT (HTM)	24.60	25.50	1.150	83.80	*n-i-p*	[40]
BTD/P3HT (HTM)	10.80	17.10	1.009	62.70	*n-i-p*	[43]
PEDOT:PSS (HTM)	3.90	10.32	0.600	63.00	*p-i-n*	[35]
PEDOT:PSS (HTM)	18.00	20.11	1.110	80.60	*p-i-n*	[36]
PDTIDTBT (HTM)	17.90	22.50	1.090	73.00	*n-i-p*	[44]
PDTPC (HTM)	16.96	21.94	1.080	71.58	*n-i-p*	[45]
PPY2 (HTM)	22.41	23.56	1.160	82.00	*p-i-n*	[46]
PMMA-CNT (HTM)	21.70	23.30	1.160	79.80	*p-i-n*	[47]
N2200 (ETM)	8.15	14.70	0.840	66.00	*n-i-p*	[50]
PNVT-8 (ETM)	7.13	13.53	0.850	62.00	*n-i-p*	[50]
PNDI2OD-TT (ETM)	6.11	13.71	0.810	55.00	*n-i-p*	[50]
PFN-2TNDI (ETM)	16.70	21.90	0.980	78.00	*p-i-n*	[51]
P(NDI2DT-TTCN) (ETM)	17.00	22.00	1.000	77.40	*p-i-n*	[52]
PFPDI (ETM)	15.01	23.43	0.963	66.50	*p-i-n*	[22]

4. Polymers as an interfacial layer

Interface engineering impact the performance and stability of PSCs, as these factors strongly depend on the interaction between the perovskite layer and adjacent HTM or ETM or between electrodes and HTM/ ETM. It is proposed that making a water-resistant polymeric layer can protect the perovskite layer from corrosion by water or moisture.[53] The structure and summary of some polymers as an interface are also presented in **Scheme 2** and **Table 2**, respectively.

4.1. Perovskite/HTM interface

Malinkiewicz *et al.* in 2014 employed poly(*N,N'*-bis(4-butylphenyl)-*N,N'*-bis(phenyl)benzidine) (polyTPD) into the perovskite/PEDOT:PSS with a PCE of 12%

that was a respected power conversion efficiency at that time.[54] Meng *et al.* used low-cost and stable conjugated polymer poly[(thiophene)-alt-(6,7-difluoro-2-(2-hexyldecyloxy)quinoxaline)] (PTQ10) as a hole extracting and cation-preserving interlayer in regular planar PSC. The introduction of PTQ10 between PTTA as an HTM and perovskite layer not only achieve high performance with PCE of 21.20% but also showed thermal and ambient stability.[55] Akman and Akin investigated the dual-functional of poly (*N,N*′-bis-4-butylphenyl-N,N′-bisphenyl)benzi-dine (PolyTPD) as HTM and interfacial passivating agent. Poly-TPD exhibited moderate efficiency of 15.60% as an HTM, with considerable stability in comparison with traditional HTM, spiro-MeOTAD, owing to its hydrophobic and hydrophilic characteristics. PolyTPD is not only utilized as HTM but also introduced in PSCs as an interfacial passivator for perovskite and grain boundaries by preventing the penetration of degradation agents into inner layers. PolyTPD also promotes hole transportation and reduces charge-carrier recombination resulting in a high PCE of 21.37% with excellent operational stability (~95% retention after 800 h).[56] Modification of NiO_x with PTAA, PMMA, and PS induces efficient charge transport between perovskite/HTM and reduced energy loss at the interface, as well as energy level alignment with the perovskite materials. The NiO_x-PTAA, NiO_x-PMMA, and NiO_x-PS based PSC exhibited PCE of 21.56%, 21.08%, and 20.84%, respectively with a V_{oc} as high as ~1.19 V listed as one of the highest V_{oc} for NiO_x-based inverted PSCs.[57] Tavakoli *et al.* deposited a thin layer of PMMA,[44] at the perovskite/HTM interface and measured PCE of 19.89%.

4.2. Perovskite/ETM interface

Different polymeric interlayers are employed between perovskite and ETM to enhance PSC's performance. Teflon, polyvinylidene-trifluoroethylene copolymer (PVDF-TrFE), and polystyrene (PS) have been successfully used as insulating tunneling layers between C_{60} as ETM and the active perovskite film to prevent perovskite layer from moisture damage. Relative to the control device, the performance of the PSCs increased significantly from PCE of 16.90% for the control PSC (PCBM) to 20.30% by employing a 1.0% PS solution.[53] NDP-V, in addition, to being used as ETM in inverted PSCs can also be sandwiched between perovskite and C_{60} as ETM. The introduction of the NDP-V interlayer showed a significant improvement with a PCE of 19.09%, surpassing the control PSC that measured 17.09% (C_{60}-based ETM).[49] According to the passivation effect of PS, Wu *et al.* fabricated dual-side passivated PSCs by introducing a PS layer between both the perovskite/SnO_2 and perovskite/HTM interface. The PS buffer layer

not only improves the efficiency of PSC with a PCE of 21.89% but also improves device stability by preventing moisture (**Fig. 5**).[58]

Similarly, poly[(9,9-bis(3-((*N,N*-dimethyl)-*N*-ethyl-ammonium)-propyl)-2,7-fluorene)-alt-2,7-(9,9-dioctylfluorene)]di-iodide (PFN-I) was introduced as a promising interface at both the perovskite/polyTPD and perovskite/ PCBM to achieve long-term stability with a PCE up to 20.56%.[59]

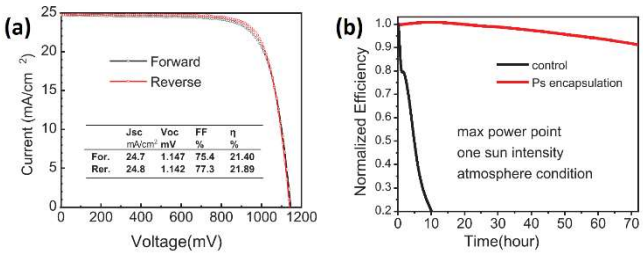

Fig. 5. a) J–V curves, b) Stability test under the 100 mW cm−2 illumination (LED) in an ambient atmosphere (25 °C, 25 RH%) for the control and PS inner-encapsulated devices.58 Copyright 2019, Wiley-VCH.

4.3. Electrode/ HTM or ETM interface

The contact resistance between electrodes and the organic CTMs has a significant effect on the electrical properties of the device causing poor electron injection and extraction. The interface layer either can be inserted into perovskite/HTM, perovskite/ ETM, or can be placed between charge transport materials/electrode interface to enhance the performance and stability of the device. Incorporation of poly(ethylenimine) ethoxylated (PEIE) or poly[3-(6-trimethylammoniumhexyl) thiophene] (P3TMAHT) as a polyelectrolyte interlayer between PCBM and Ag electrode in inverted PSC promoted the performance of the device to reach the PCE of 12.01, and 11.28%, respectively as compared with the control PSC without

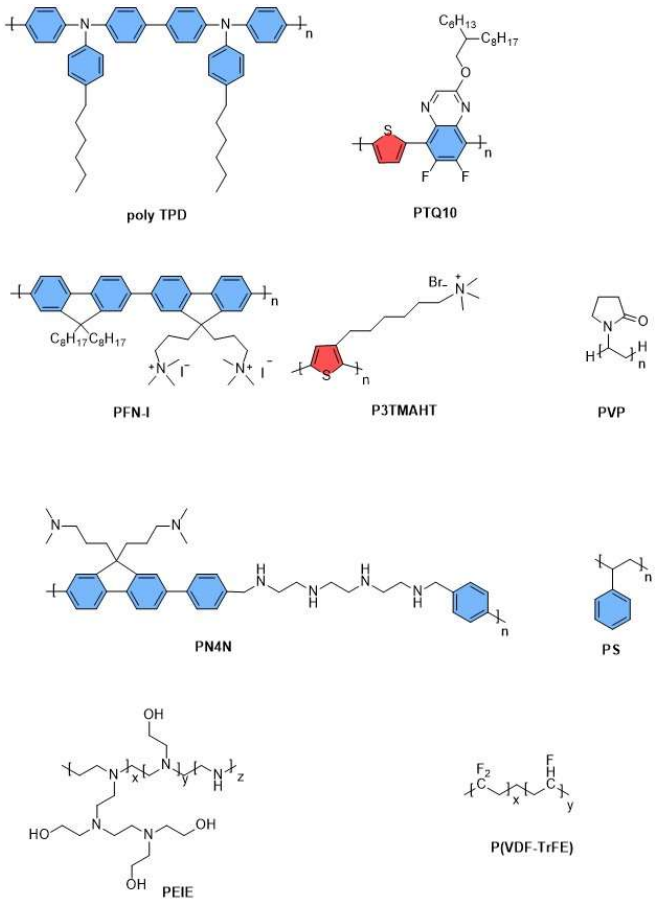

Scheme 2. The structure of polymers as interface materials.[53–55,59–62]

interlayer (PCE of 8.53%). Polymer interlayer reduced the electron injection resistance to PCBM from 7.96 Ω cm^2 to 1.00 Ω cm^2 (PEIE) and 0.99 Ω cm^2 (P3TMAHT).[60] PN4N, an amino-functionalized polymer as a cathode interlayer could reduce the contact resistance, block interfacial charge recombination, and enhance electron transport, resulting in an improvement of efficiency from PCE of 12.40% to 15.00%.[61] In addition, to modification of PSCs, poly(vinylpyrrolidone) (PVP) has been also inserted between the Ag cathode and PCBM, leading to lower interfacial resistance, better electron transportation, as well an improvement of FF from 58.98% to 66.13%, and the PCE increases from 10.83% to 12.55%.[62] Sun *et al*. introduced a high-performance device with a certified PCE of 21.44% and negligible hysteresis through the deposition of a double-layered ETM consisting of (PEIE)/SnO_2 composite in contact with an ITO electrode. The ultrathin polyelectrolyte PEIE interlayer was interfaced with ITO and the SnO_2 layer was in contact with the perovskite layer which could control nucleation and reduce the energy mismatch between the PEIE/SnO_2 composite ETM and perovskite.[63]

Table 2. Photovoltaic performance of PSCs by using some polymeric interface

Polymeric interface	PCE [%]	J_{sc} [mA cm^{-2}]	V_{oc} [V]	FF [%]	Device structure	Ref.
PolyTPD (PSK/ HTM)	12.04	16.12	1.050	67.00	*p-i-n*	[54]
PTQ10 (PSK/HTM)	21.20	23.15	1.120	81.57	*n-i-p*	[55]
PolyTPD (PSK/HTM)	21.37	23.30	1.167	79.00	*n-i-p*	[56]
PTAA(PSK/HTM)	21.56	22.23	1.190	81.71	*p-i-n*	[57]
PMMA(PSK/HTM)	21.08	22.23	1.190	78.61	*p-i-n*	[57]
PS(PSK/HTM)	20.84	22.38	1.170	79.47	*p-i-n*	[57]
PMMA (PSK/HTM))	19.89	22.60	1.140	77.20	*n-i-p*	[44]
PS (PSK/ETM)	20.30	22.90	1.100	80.60	*p-i-n*	[53]
NDP-V (PSK/ETM)	19.09	22.11	1.062	81.00	*p-i-n*	[49]
PS (PSK/ETM, PSK/ HTM)	21.89	24.80	1.142	77.30	*n-i-p*	[58]
PFN-I(PSK/ETM, PSK/ HTM)	20.56	22.48	1.130	81.00	*p-i-n*	[59]
PEIE (ETM/Ag cathode)	12.01	17.32	0.899	77.10	*p-i-n*	[60]
P_3TMAHT (ETM/Ag cathode)	11.28	17.10	0.899	74.10	*p-i-n*	[60]
PN4N (ETM/Al cathode)	15.00	20.61	1.000	72.50	*p-i-n*	[61]
PVP (ETM/Ag cathode)	12.55	16.96	0.960	66.13	*p-i-n*	[62]
PEIE (ITO/ETM)	21.44	24.34	1.120	78.64	*n-i-p*	[63]

5 Polymers as an additive

5.1. Polymeric additives into perovskite

Polymers as additives into the perovskite layer provide a tool to promote device efficiency, stability, and film quality of perovskite layers like crystallinity, morphology, and coverage. At the initial step, poly(2-ethyl-2-oxazoline) (PEOXA) was inserted into the $CH_3NH_3PbI_3$ to control the crystallization process and structure of the perovskite layer. A PCE up to 6.35% was achieved by adding a small percentage (1.5 wt%) of PEOXA into the perovskite layer.[64] Since then, several attempts have been made to improve the performance of the device by adding polymers into the active layer. Tuning the morphology of perovskite by polyethylene glycol (PEG) as an additive resulted in lower voids between perovskite domains and better coverage of perovskite film on the TiO_2 layer. By utilizing 1 wt% of PEG more than 25% of improvement was obtained from PCE of 10.58% to 13.20%.[65] PMMA as an efficient template to control nucleation and crystal growth [24] of the perovskite layer resulted in PCE of up to 21.60% (**Fig. 6**). Zhao *et al.* utilized a polymerization-assisted grain growth (PAGG) strategy to obtain high stability and high-performance device with a PCE of 23.00%. The incorporation of dimethyl itaconate (DI) as a sufficient monomer into the PbI_2 solution formed the

perovskite layer, where, the polymers adhered at the perovskite grain boundaries making effective passivation resulting in low defect density.[66] The structure and summary of some polymeric additives are presented in **Scheme 3** and **Table 3**, respectively.

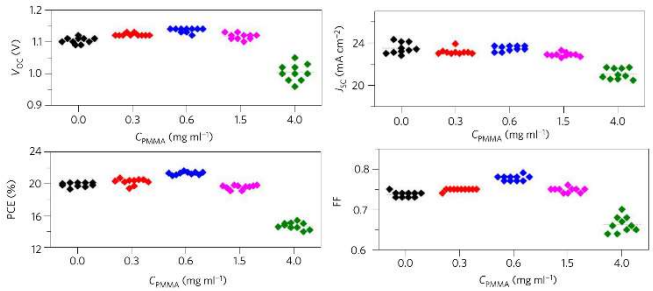

Fig. 6. Photovoltaic performance of devices plotted as a function of PMMA concentrations (CPMMA, mg ml−1), the data points with the same color correspond to the same PMMA concentration.24 Copyright 2016, Nature.

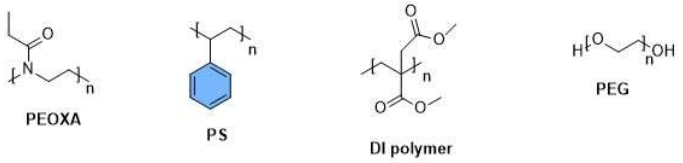

Scheme 3. The structure of polymeric additives. [64–68]

5.2. Polymeric additives into HTM

Habisreutinger *et al.* incorporated a P3HT-SWNT layer in-filled with insulating polymer PMMA and the effect of mixed HTM on the device performance was investigated. Employing polymer-assisted single-walled carbon nanotubes (SWNTs) as HTM improved the power efficiency of perovskite solar cells up to 15.30% with a protective effect between the perovskite film and metal cathode that enhanced stability to thermal stressing and moisture ingress.[69] PTAA doping into the 4,4'-cyclohexylidenebis[*N,N*-bis(4-methyl-phenyl)benzenamine] (TAPC) layer, formed a mixed HTM with a smooth surface and energy level alignment with perovskite leading to improve charge transfer and reduce charge recombination. With this strategy highly performance PSC was developed with an average PCE of 19.03% ± 0.53%, and the highest PCE of 21.01%.[70] Addition of PEDOT:PSS as a dopant into metal-phthalocyanine−tetrasulfonated acid tetrasodium salt (TS-MPc) as the main HTM improved the cell efficiency of *p-i-n* inverted PSCs. The first report of the nano-mesh structure formation in a TS-MPc:PEDOT:PSS blended system exhibited a higher cell efficiency, power conversion efficiency (PCE) of 14.65%, V_{oc} of 0.950 V, J_{sc} of 19.861 mAcm^{-2}, and a FF of 77.64%, compared with that of both pure TS-CuPc (PCE of 7.99%)

and PEDOT:PSS (PCE of 11.02%). The stability of the device improved with PEDOT: PSS-assisted TS-MPc as HTM.[71]

5.3. Polymeric additives into ETM

As the first reported polymeric additives into PCBM as ETM, Bai *et al.* incorporated high molecular weight polystyrene (PS) into PCBM to promote ETM film quality (highly smooth and uniform ETM) resulting in a significant improvement in PCE from 9.50% to 10.68% at 1.5 wt% PS doped PSC.[67] To fabricate a cost-effective and simple device PEG was incorporated into colloidal-quantum-dot ink (SnO_2) as ETM. Dissolving PEG into SnO_2 ink fabricates a dense and uniform SnO_2-in-polymer matrix (SPM) layer with thickness below 20 nm measuring a high PCE of 20.80% with V_{oc} of 1.12 V and FF of 81.90%.[68]

Table 3. Photovoltaic performance of PSCs by using some polymeric additives

Polymer	PCE (%)	J_{sc} (mA cm^{-2})	V_{oc} (V)	FF (%)	Device structure	Ref.
PEOXA (into PSK)	6.35	8.95	1.070	66.00	*p-i-n*	[64]
PEG (into PSK)	13.20	19.53	0.940	70.35	*n-i-p*	[65]
PMMA (into PSK)	21.60	23.70	1.140	78.00	*n-i-p*	[24]
DI polymer (into PSK)	23.00	24.90	1.145	80.60	*n-i-p*	[66]
P3HT, PMMA (into HTM)	15.30	22.71	1.020	66.00	*n-i-p*	[69]
PTAA (into HTM)	21.01	23.43	1.120	80.14	*p-i-n*	[70]
PEDOT:PSS (into HTM)	14.65	19.86	0.950	77.64	*p-i-n*	[71]
PS (into ETM)	10.68	15.62	1.070	64.00	*p-i-n*	[67]
PEG (into ETM)	20.80	22.67	1.120	81.90	*n-i-p*	[68]

Polymers to improve stability

The perovskites are very sensitive to moisture and degrade in the ambient environment. Poor stability of PSCs under moisture conditions is an obstacle to their practical applications. Device degradation not only takes place through moisture but also through heat and UV irradiation.[72] Different efforts have been made to improve the stability of PSCs. As an alternative approach adding polymer additives, and interface engineering are promising routes to improve device stability. The structure and summary of some polymers to improve the stability are also presented in **Scheme 4** and **Table 4**, respectively. For example, hygroscopic PEG can stabilize the perovskite layer making

PEG-scaffold PSC with strong humidity resistance. The modified device exhibited high output even in 70% RH for over 300 h.[73] The introduction of polyethylene oxide (PEO) into the active layer can improve the humidity tolerance in a moisture processing environment (55±5% RH). The fabricated device in high humidity (55±5% RH) exhibited a PCE of 11.70% compared to that fabricated in a dry environment (30±5% RH), while the devices without PEO, fabricated in high moisture and dry moisture showed a significant difference in performance.[74] Moreover, fabrication of dopant-free HTM by random copolymer (RCP) based on benzo[1,2-b:4,5:b']dithiophene (BDT) and 2,1,3-benzothiadiazole (BT) as HTM, resulted in a radically stable device even at 75% RH for over 1400 h with PCE of 17.30% (**Fig. 7**).[75]

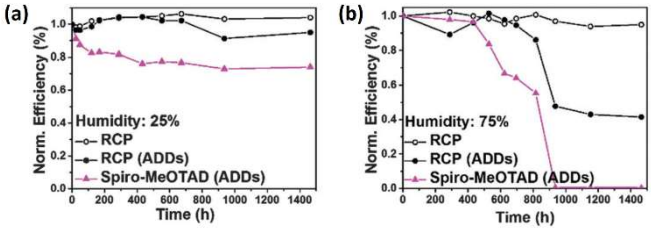

Fig. 7. (a) Stability test at 25% humidity, (b) the stability test at 75% humidity.[75] ADDs: Additives (lithium bis(trifluoromethanesulfonyl)imide (LiTFSI) and tert-butylpyridine (t-BP)) Copyright 2016, Royal Society of Chemistry.

Dai *et al.* showed P3HT doped into PCBM (ETM) as an additive that can improve the aggregation of PCBM and modify the surface morphology of ETM, leading to improve ETM stability. The P3HT introduction protects the perovskite layer from water diffusion, leading to humidity resistance. As a result, the device based on the P3HT/PCBM (1:30) exhibited an impressive PCE of 20.84% with a J_{sc} of 23.27 mA/cm^{-2}, V_{oc} of 1.10 V, and a FF of 81.47%. The PCE of device retained 85.03% for 720 h (20% RH), 77.90% for 48 h (60% RH), 44.31% for 1 h (90% RH), and 17.43% for 30 min (in water) of its initial PCE value. Moreover, by the introduction of P3HT, the J_{sc} exhibited almost no degradation at first 360 h exposure and retained 91.41% of its initial value after 720 h, while the J_{sc} of the control device decayed after 120 h and retain 86.94% of the initial value after 720 h.[76]

The introduction of electron-poor moieties into P3HT not only improved charge transport properties due to more efficient intramolecular interactions but also lead to more stability.[77,78] Employing modified P3HT by benzothiadiazole (BTD-modified P3HT) as HTM in flexible PSC could improve the charge mobility through the HTM

due to having a donor-acceptor behavior. De Rossi *et al.* demonstrated improved device stability with BTD-P3HT copolymers as compared to commercial P3HT and Spiro-OMeTAD. Moreover, the fabricated device by polymeric BTD/P3HT exhibited a performance comparable to the commercially P3HT.[43]

The addition of PANI with unique optical and electrical properties into perovskite film not only improved stabilities against heat (retained 86% of absorption intensity after 200h of heat aging) and moisture (larger water contact angle, 71.7^{o}, than the pristine device, 62.1^{o}) but also improved light absorption, charge transfer, morphology and crystalline structure of the film. Subsequently, the performance of the modified device improved and gave a PCE of 19.09%.[79] Porphyrin derivatives with champion thermal stability are largely used in photovoltaic devices. With the introduction of polymeric zinc porphyrin $(ZnP)_n$, stabilities against heating (retained 77% of intensity after 900h at 85^{o}C) and lighting (retained 86% of intensity after 630 h under the white LED) improved, and the PCE of the device also increased to 20.53%.[80] Moreover, through the polymerization-assisted grain growth (PAGG) method dimethyl itaconate (DI) was polymerized, chemically gathered at the perovskite grain boundaries, the main channels for moisture penetration into the perovskite layer, and effectively reduced the defects accumulated at the grain boundary area. PAGG treated solar cells resulted in superior stability and performance (PCE of 23.00%), where 85.7% and 91.8% of the initial PCE were retained after 504 h continuous illumination and 2208 h shelf storage in ambient conditions, respectively.[66] Employing hydrophobic and cross-linkable ethyl 2-cyanoacrylate (E2CA) into the active layer not only increases heat resistance (retained over 90% of the post-burn-in efficiency after 200 h) and humidity resistance (retained about 90% of the efficiency after aging over 1000 h in 40-60% RH) but also decreased the polymerization temperature without damaging active layer (**Fig. 8**).[81]

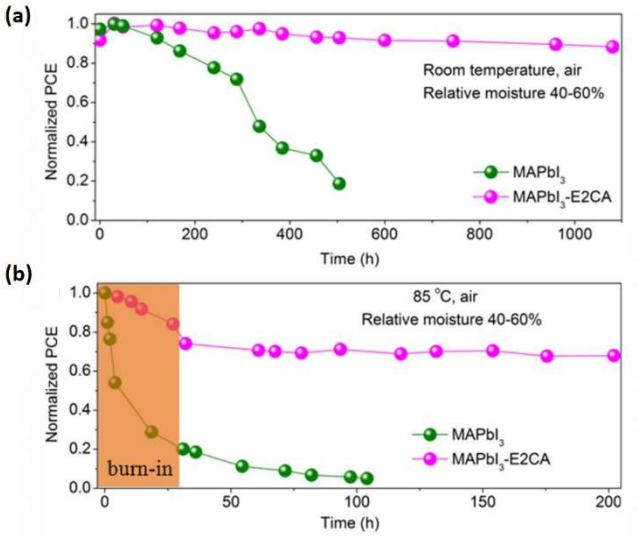

Fig. 8. (a) Moisture stability of PSCs stored in air (relative humidity: 40-60%). (b) Thermal stability of PSCs stored at 85 °C in air (relative humidity: 40-60%).[81] Copyright 2019, Elsevier.

7. Use of polymers to minimize the V_{oc} *deficit*

Interfacial engineering can improve V_{oc} by improving charge transport, trap density reduction, and preventing non-radiative recombination. The modification of PSCs by polymers is a significant approach to improve V_{oc} and device performance. The structure and summary of some polymers to improve V_{oc} is also presented in Scheme 4 and Table 4, respectively. Lian *et al.* showed modification of NiO_x by PTAA in inverted PSCs could improve the device PCE to 21.56% with a V_{oc} of 1.19 V.[57] Placement of a thin PMMA/PCBM blend film into the active layer/TiO_2 interface suppressed interfacial recombination resulting in an increase in V_{oc} by as much as 80 mV. The efficient passivated device exhibited a significant V_{oc} of 1.18 V with a steady-state PCE of 20.40% as well as negligible hysteresis.[82] Interface passivation by the introduction of PMMA at both active layer/HTM and active layer/ETM interface successfully could reduce interface recombination. As a result, a remarkable V_{oc} of 1.22 V with high efficiency of 20.80% was achieved.[83] Moreover, the band alignment of the perovskite with HTM is essential for increasing $V_{oc.}$ The incorporation of fluorine atoms as an electron-withdrawing group (EWG) into PTAA resulted in a deeper HOMO energy level. The alignment energy level of fluorinated PTAA (F-PTAA) with perovskite film could improve the performance of the device with a V_{oc} of 1.14 V and PCE of 21.10%.[84]

8. Polymeric materials to improve FF

FF is a measure of the quality of solar cells and it is a ratio of the maximum power of the device to the product of V_{oc} and J_{sc}. The ideal FF should be 100% but experimentally, it is not possible. Several works introduce polymers to improve FF. The structure and

summary of some polymers to improve FF is also presented in **Scheme 4** and **Table 4**, respectively. For example, PTAA as an HTM can improve the FF of PSCs. Wang *et al.* by using an ultrathin PTAA sandwiched between the active layer and PEDOT:PSS effectively passivated the interfacial and grain boundary defects, and suppress interfacial recombination. As a result, they obtained a PCE of 19.04% with a striking FF of 82.59% and a J_{sc} of 21.38 mA cm-^{2}.[85] Moreover, using Zn-doped PEDOT:PSS as HTM improved the photovoltaic performance, where the FF increased from 70.00% to 83.00%.[86] Introduction of low-cost and stable conjugated polymer like poly[(thiophene)-alt-(6,7-difluroro-2-(2-hexyldecyloxy)-quinoxaline)] (PTQ10) as an interfacial layer in planar *n-i-p* PSC not only improve active layer quality, and suppress the volatilization of organic cations during the thermal annealing process, but also function as a hole selective layer. As a result, a champion PCE of 21.20% with a high FF of 81.60% as well as thermal and ambient stability was achieved.[55] Also, poly aspartic acid sodium (PASP), an interlayer between HTM and active layer, passivate surface traps in perovskites and control the crystallization, resulting in high device performance with a champion PCE of 20.05% as well as a high FF of 82.20%.[87] Introduction of conjugated n-type polymer, poly[(9,9-dioctyluorene)-2,7-diylalt-(4,7-bis(3-hexylthien-5-yl)2,1,3-benzothiadiazole)-2',2''-diyl] (F8TBT), into PCBM as ETM could controlled active layer formation, enhanced electron mobility, and reduced recombination at perovskite/PCBM interface. As a result, device performance with PCE of 20.60% and FF of 82.00% as well as high stability (remaining 80% of efficiency after 45 days under ambient air condition) was achieved.[88]

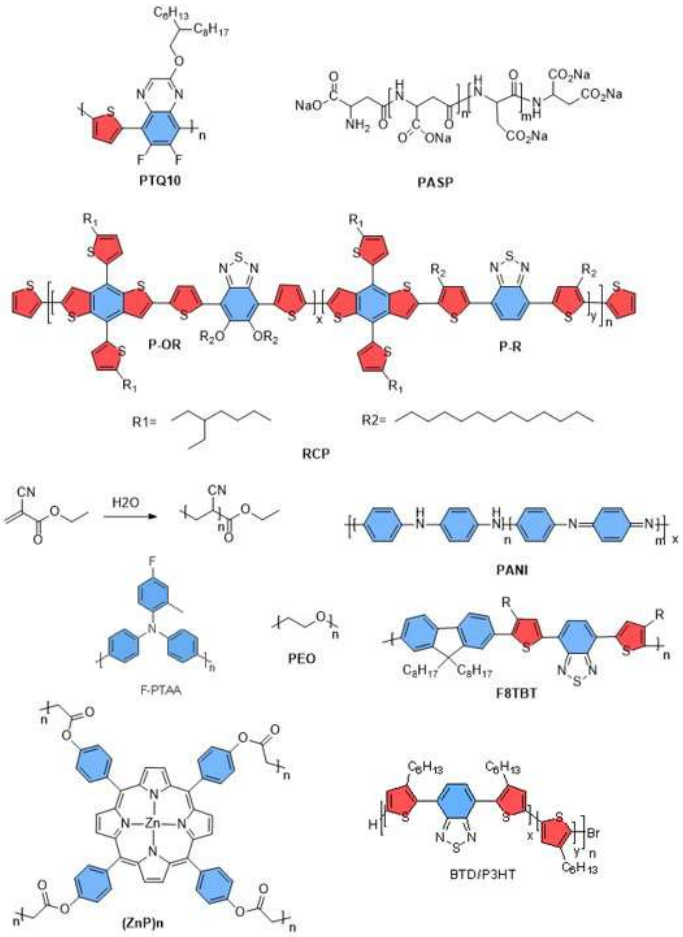

Scheme 4. The structure of polymers to improve stability, V_{oc}, and FF.[43,55,74,75,79–81,84,87,88]

Table 4. Photovoltaic performance of PSCs by using some polymers to improve stability, V_{oc}, and FF

Polymer	PCE%	J_{sc} (mA cm^{-2})	V_{oc} (V)	FF%	Device structure	Ref.
PEG	16.00	22.50	0.980	72.00	*n-i-p*	[73]
PEO	11.70	16.80	0.920	75.70	*p-i-n*	[74]
RCP	17.30	21.90	1.080	75.00	*n-i-p*	[75]
P_3HT	20.84	23.27	1.100	81.47	*p-i-n*	[76]
BTD/P3HT	10.80	17.10	1.009	62.70	*n-i-p*	[43]
PANI	19.09	22.50	1.100	77.13	*n-i-p*	[79]
$(ZnP)_n$	20.53	23.19	1.110	79.29	*p-i-n*	[80]
Polymeric DI	23.00	24.90	1.145	80.60	*n-i-p*	[66]
Polymeric E2CA	21.03	23.02	1.120	81.40	*p-i-n*	[81]
PTAA	21.56	22.23	1.190	81.71	*p-i-n*	[57]
PMMA	20.40	23.10	1.160	76.20	*n-i-p*	[82]
PMMA	20.80	22.60	1.213	76.00	*n-i-p*	[83]
F-PTTA	21.20	23.40	1.140	82.30	*n-i-p*	[84]
PTAA	19.04	21.38	1.070	82.59	*p-i-n*	[85]
Zn-dopped PEDOT:PSS	13.20	17.20	0.925	83.00	*p-i-n*	[86]
PTQ10	21.20	23.15	1.120	81.57	*n-i-p*	[55]
PASP	20.05	22.80	1.070	82.20	*p-i-n*	[87]
F8TBT	20.60	22.43	1.120	82.00	*p-i-n*	[88]

9. Synthesis of polymeric materials

The functionalized PTAA (CH_3O-PTAA, CH_3-PTAA, and F-PTAA) were synthesized through the modified Ni-catalyzed Yamamoto polycondensation reaction [89] by the desired monomers from Buchwald-Hartwig amination, as outlined in **Scheme 5**. The obtained polymers were purified by filtration through a short bed of silica gel, followed by Soxhlet extraction, collected by precipitation into methanol, filtered, and dried under vacuum.[29,84] The Suzuki polycondensation is another route for the preparation of functionalized PTAA (**Scheme 5**). Based on the results the obtained polymeric HTM improved the photovoltaic properties of the cell compared with commercial PTAA, suggesting the synthetic method is a very important issue to obtain a high-performance device.[30]

PDTPC with the donor and acceptor units namely dithienopicenocarbazole (DTPC) and fluorinated benzothiadiazole (F-BT) was obtained via Suzuki coupling polymerization as outlined in **Scheme 6**.[45] Moreover, the amino-functionalized polymers PFN-2TNDI and PN4N were synthesized by Suzuki copolymerization from desired boronic ester and

aryl halide (**Scheme 6**). On the other hand, the Sonogashira cross-coupling reaction was applied for the preparation of PPY2 in presence of a palladium catalyst, a copper (I) cocatalyst, and an amine base as described in **Scheme 6**.

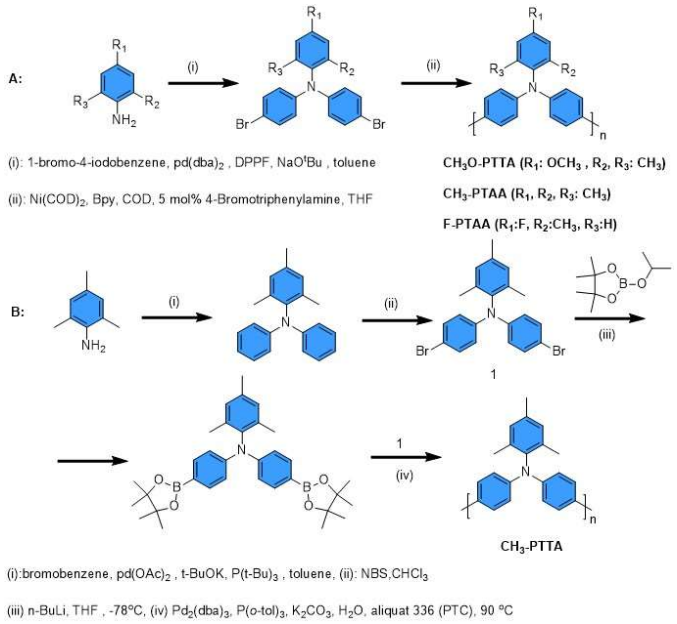

Scheme 5. Synthetic routes of functionalized PTAA, A: Yamamoto polycondensation 89, Reproduced from Ref. 89, Copyright 2009, Nature Publishing Group. B: the Suzuki polycondensation.30 Reproduced from Ref. 30, Copyright 2020, Elsevier.

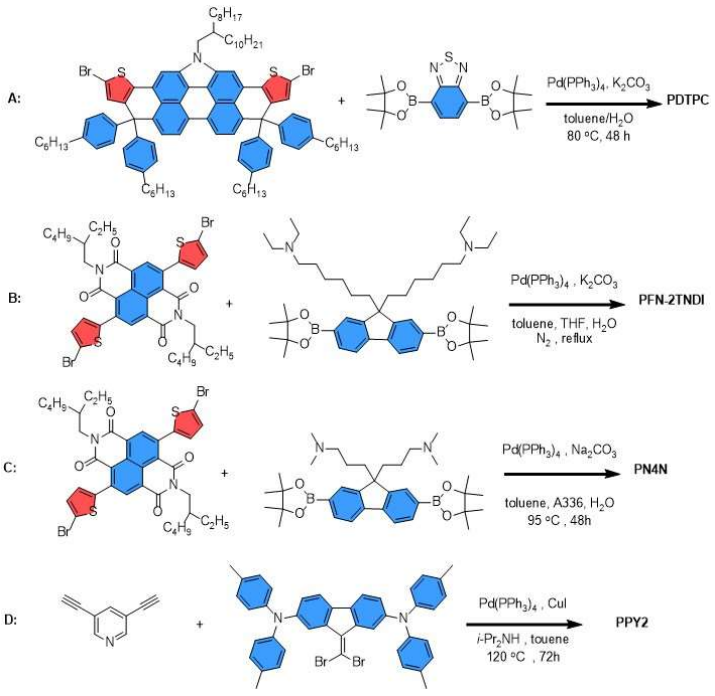

Scheme 6. Synthetic routes of (A): PDTPC, (B) PFN-2TNDI, (C) PN4N, and (D): PPY2 by cross-coupling reaction.45 Reproduced from Ref. 45, Copyright 2021, American Chemical Society.

The reaction of 2-bromo-3-hexylthiophene with lithium diisopropylamide (LDA), MgBr, and then 1,3-bis(diphenylphosphino)propane nickel (II) chloride (Ni(dppp)Cl_2)

can result in highly regioregular P3HT [90–92] through Grignard type polycondensation reaction (**Scheme 7**). De Rossi *et.al.*[43] synthesized different BTD/P3HT copolymers by Stille coupling [78] and Kumada polycondensation[93] reactions. Through the Stille coupling reaction, the BTD/3-hexylthiophene (HT) ratio could be controlled, whereas by Kumada reaction a polymer with relatively high molecular weight has been achieved. Due to the low M_w of the former (by Stille coupling) low FF and low efficiency were achieved, while the other one (by Kumada reaction) demonstrated improved stability and efficiency. The polymerization of corresponding monomers through the Kumada reaction is illustrated in **Scheme 7**.

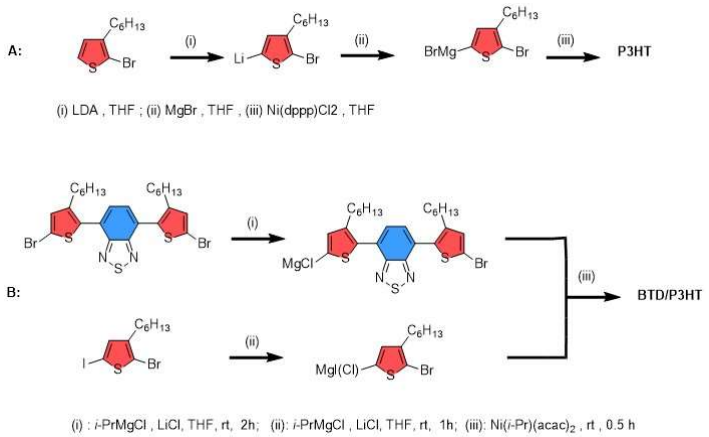

Scheme 7. Synthetic routes of (A): P3HT[94], Reproduced from Ref. 94, Copyright 1998, American Chemical Society. (B): BTD/P3HT by Kumada polycondensation reaction.[43] Reproduced from Ref. 43, Copyright 2021, Elsevier.

PDTIDTBT [44,95] as a HTM for PSC was synthesized from Stille cross-coupling polycondensation from two monomers namely 2,7-dibromo-(5,5-bis(3′,5′-dimethyloctyl)-5H-1,8-dithia-as-indacenone) (M1) and 5,5-bi(tributylstannyl)-(5′,6′-dioctyloxy-4′,7′-di-2-thienyl-2′,1′,3′-benzothiadiazole (M2) as outline in **Scheme 8**. The growth of the polymer chain ended with the addition of 2-bromobenzene and 2-(tributylstannyl)thiophene for the appropriate time. Similarly, highly planar π-conjugated copolymer IDTB and RCP were obtained from their corresponding monomers by Stille coupling polymerization (**Scheme 8**).[9]

Stille cross-coupling condition has been also employed for the synthesis of such polymeric ETM including NDP-V, PNVT-8, N2200, (PNDI2OD)TT, and P(NDI2DT-TTCN) as described in **Scheme 9**.[49,50,52,96–101] Polymeric DI is the result of radical polymerization in the presence of azobisisobutyronitrile (AIBN) as an initiator. By the introduction of the monomeric DI into the PbI_2 solution and initiating the

polymerization process, C=C bonds of monomers are cleaved and then subsequently relinked with adjacent monomers to form polymeric DI.[66]

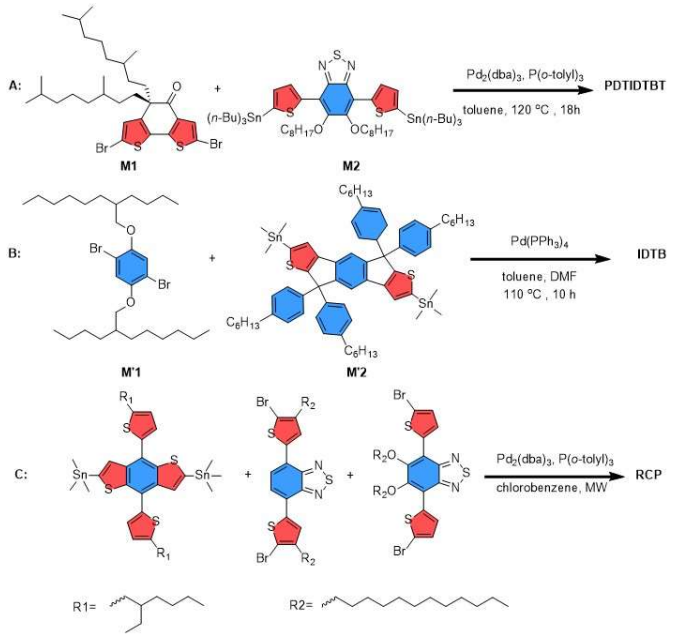

Scheme 8. Synthetic routes of (A): PDTIDTBT, Reproduced from Ref. 44, Copyright 2021, Wiley-VCH. Reproduced from Ref. 95, Copyright 2019, United States National Academy of Sciences. (B): IDTB copolymer and (C) RCP by Stille cross-coupling polycondensation, Reproduced from Ref. 9, Copyright 2020, Wiley-VCH.[9,44,95]

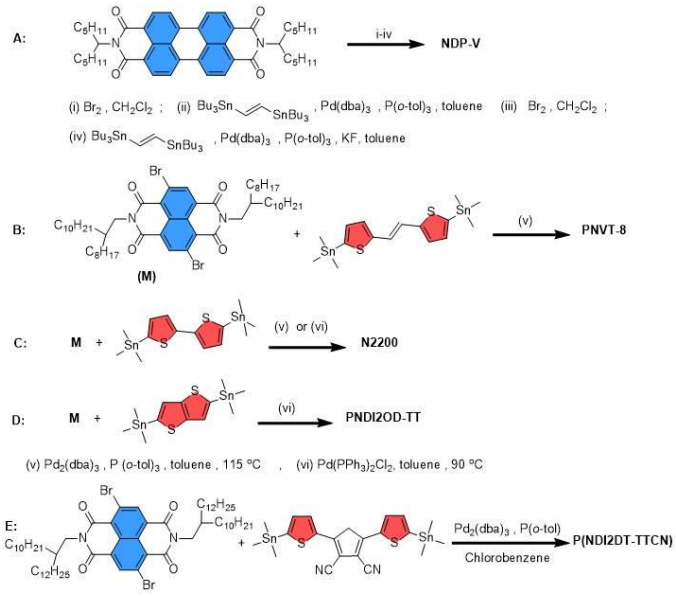

Scheme 9. Synthetic routes of (A)NDP-V, (B): PNVT-8, (C): N2200 (D): (PNDI2OD)TT and (E) P(NDI2DT-TTCN) by Stille cross-coupling polycondensation.[49,50,52,66,72,96–100] Reproduced from Ref. 49, Copyright 2018, American Chemical Society. Reproduced from Ref. 50, Copyright 2015, American Chemical Society. Reproduced from Ref. 52, Copyright 2018, Wiley-VCH. Reproduced from Ref. 66, Copyright 2020, Wiley-VCH. Reproduced from Ref. 72, Copyright 2018, Wiley-VCH. Reproduced from Ref. 96, Copyright 2017, Wiley-VCH. Reproduced from Ref. 97, Copyright 2014, American Chemical Society. Reproduced from Ref. 98, Copyright 2014, Wiley-VCH. Reproduced from Ref. 99, Copyright 2013, American Chemical Society. Reproduced from Ref. 100, Copyright 2011, American Chemical Society.

10. Characterization of polymeric materials

10.1. The NMR spectroscopy

The ^{1}H-NMR and ^{13}C-NMR analyses were used to elucidate the structure of the polymers. The ^{1}H-NMR spectra (400 MHz) of CH_3O-PTAA in *o*-dichlobezene-d4 displayed aromatic protons as one singlet at 6.89 ppm (2H) and two doublets at 7.50-7.48 (4H) and 7.09 ppm (4H) with coupling constants of 8.5 and 8.4 Hz, respectively. The singlets at 3.68 (3H) and 2.10 (6H) ppm were attributed to methoxy and methyl groups, respectively. The aromatic protons of CH_3-PTAA appeared at 7.47-7.45 (4H) and 7.09-7.07 (4H) ppm as doublets with coupling constants (*J*) of 8.5 and 8.7 Hz respectively, as well as a singlet at 6.86 ppm (2H). The protons belonging to the methyl groups appeared at 2.25 (3H) and 2.06 ppm (6H) as singlets.[29] The ^{1}H-NMR spectra of F-PTAA displayed aromatic protons at 7.42-7.40 ppm as a doublet (4H, *J*= 9.0 Hz) and at 7.15-7.13 (1H) and 7.02-6.90 ppm (6 H) as a multiplet, while methyl group appeared as a singlet at 2.07 ppm.[84] The ^{1}H-NMR spectra of BTD/P3HT displayed the thiophene proton in the 4-position on the ring at 6.98 ppm. Since the chemical shift of the α-methylene group is affected by the chemical environment and regio-regularity,[102] the narrow peak belonging to the α-methylene group at 2.8 ppm suggests the high regioregularity of the copolymer and is estimated to be about 100%.[43] PDTIDTBT is synthesized by Stille cross-coupling polycondensation and characterized by the ^{1}H-NMR technique (400 MHz) in deuterated chloroform. The aromatic protons appeared as broad signals at 7.8-7.5 (1H), 7.4-7.3 (4H), and 7.2-7.0 ppm (1H), and the aliphatic ones at 4.4-4.1 and 2.3- 0.6 ppm.[44] To note here, we believe this compound has 76 aliphatic protons, however, the report suggests 60 aliphatic protons. Synthesis of IDTB copolymer was also monitored by ^{1}H-NMR spectroscopy (600MHz, $CDCl_3$). The signals at 7.51 (s, 2H), 7.41 (s, 2H), 7.19-7.05 (18H) were attributed to aromatic protons and the other ones at 4.03-3.76 (m, 4H), 2.68-2.39 (m, 8H), 1.81 (s, 2H), 1.66-1.41(m, 8H), 1.39-1.12 (m, 56H), 0.97-0.71 (m, 24H) were assigned to aliphatic chain protons.[9] The aromatic protons of PPY2 appeared at 8.47-8.09 (m), 7.69-7.65 (m), and 7.12-6.89 ppm (m), while CH_3 protons appeared at 2.17 ppm as a broad signal. Moreover, ^{13}C-NMR confirmed the synthesis of brown solid PPY2. The aromatic carbons are observed between 147.43-119.58 ppm and the signal at 20.82 ppm is assigned to methyl moiety.

The ^{1}H-NMR studies suggest that PPY2 displays coordination ability to Pb^{2+} due to its outward orientation which caused the passivation ability.[46] Moreover, the synthesis of PFN-2TNDI,[51] RCP,[75] N2200,[98,99,101] PNVT-8,[99], and P(NDI2DT-TTCN) [52] was established by this technique.

10.2. Fourier-transform infrared (FTIR) spectroscopy

FTIR is a widespread technique that can play a role as the fingerprint of materials. That is one of the most applicable methods that is used to detect functional groups and structures of compounds.[103] FTIR was collected in DI and DI-PbI_2 films before and after the annealing process to verify the polymerization of DI. The pure DI exhibited the characteristic bands of C=O (stretching mode, 1737 cm^{-1}), C=C (stretching mode, 1636 cm^{-1}), and =CH_2 (bending mode, 898 cm^{-1}) groups, which retain in PbI_2 film with DI. After thermal treatment of DI-PbI_2 film, the bans related to C=C and =CH_2 moieties both disappear, indicating complete polymerization (**Fig. 9**).[66]

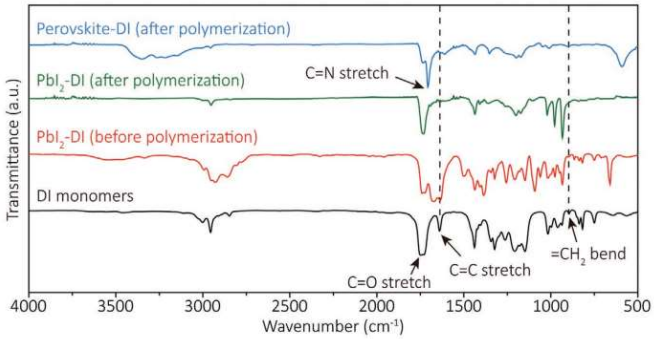

Fig. 9. The FTIR of the DI monomers, PbI_2–DI film before and after the polymerization process, and perovskite film after the intermolecular exchanging process.[66] Copyright 2020, Wiley, Wiley-VCH.

10.3. Molecular weight analyses

The molecular weight and its distribution are determined by size exclusion chromatography (SEC) and gel permeation chromatography (GPC) techniques. The number-average molecular weight (M_n) of CH_3O-PTAA, CH_3-PTAA, and F-PTAA measured by the SEC technique is 14.0, 14.1, and 25.0 $kg.mol^{-1}$ (kDa) with polydispersity values of 1.63, 1.54, and 1.90, respectively.[29,84] Further, the GPC technique was also used for CH_3-functionalized PTAA by Suzuki polycondensation reaction, and an average molecular weight of 20.8 kDa, as well as a narrow molecular weight distribution (1.4), was obtained as compared to commercial PTAA.[30] GPC analysis exhibited a relatively high molecular weight equal to 45 kDa with a dispersity of 1.25 for BTD/P3HT copolymer.[43] The average molecular weights (M_w) of PDTIDTBT and IDTB estimated by the GPC technique are 135.5 and 35.9 kDa. The

measured M_n of 67.3 and 18.3 kDa with a polydispersity of 2.0 and 1.9, respectively.[9,44] The PDTPC and PPY2 exhibited the M_n of 11.4 and 7.7 kDa with a polydispersity of 1.69 and 1.90 by GPC, respectively.[45,46]

10.4. Thermal stability

The thermal stability of polymers is evaluated by thermogravimetric analysis (TGA) and differential scanning calorimetry (DSC). TGA of PTAA derivatives by Kim *et al.* confirmed their high thermal properties with decomposition temperature (T_d) of 475, 502, and 522 ºC for CH_3O-PTAA, CH_3-PTAA, and F-PTAA, respectively. The results indicated fluorination into the polymer backbone improved thermal stability.[29,84] BTD-P3HT copolymers synthesized through Kumada polycondensation reaction exhibited T_d of 479 ºC, while T_d of commercially P3HT (94 kDa) was 485 ºC. It seems BTD moieties could reduce the thermal stability of the polymer.[43] PDTIDTBT and IDTB copolymers were also stable below 300 ºC. Thermal analysis of PDTIDTBT and IDTB under N_2 atmosphere exhibited high T_d of 324 and 376 ºC, respectively.[9,44] TGA and DSC methods were performed to investigate the thermal stability of PDTPC and PPY2 copolymers and suggest thermal stability of copolymers with 5% weight loss at 381 and 459 ºC, respectively.[45,46]

10.5. Optical and electrochemical properties

The optical and electrochemical properties of polymers were measured by different techniques such as UV-vis spectroscopy, cyclic voltammetry (CV), ultraviolet photoelectron spectroscopy (UPS), photoelectron spectroscopy in the air (PESA), and photoluminescence (PL) analysis.

The light absorption properties of polymers are influenced by conjugation length, regioregularity, planarity, and molecular weight.[43,94,104] The maximum absorption (λ_{abs}) of BTD/P3HT copolymer was at 453 nm.[43] The UV-vis absorption spectra displayed λ_{abs} peak of CH_3O-PTAA at 381 nm, whereas λ_{abs} of CH_3-PTAA appeared at 377 nm with a red-shift of about 4 nm. The maximum absorption of F-PTAA with EWG slightly decreases and shifted to the shorter wavelength (372 nm).[29,84] The maximum absorption (λ_{abs}) for PDTPC in chlorobenzene appeared at 657 nm, however, two extra signals appeared in solution form, one at 539 nm due to localized π-π* transition and the other at 657 nm related to intramolecular charge transfer between donor and acceptor units. The λ_{abs} of PDTPC in thin-film form appeared at 696 nm with a shoulder.[45] The red shifting of 39 nm can be ascribed to the enhanced order of inter-and intramolecular stacking in the solid state.[45,105,106] The optical absorption spectra of PFN-2TNDI film

exhibited two unique signals at 383 and 612 nm resulting from π-π* transition and strong intramolecular charge transfer properties of this copolymer, respectively.[51]The charge transfer properties of polymers were investigated by the photoluminescence (PL) measurements. The PL emission (λ_{em}) peak of CH_3O-PTAA (424 nm) was red-shifted from that of CH_3-PTAA (419 nm).[29] By UV and PL data Tavakoli *et al.* calculated the optical bandgap of about 1.82 eV for PDTIDTBT copolymer.[44] The PL lifetime of deposited perovskite with NDP-V (11.08 ns) confirmed that the electron extraction from perovskite to NDP-V ETM is even more effective than to PC61BM.[49]

The charge mobility was measured by the space charge limited current (SCLC) method. The hole mobility could improve by inter-and intramolecular interactions and increase in polymer backbone planarity, as an example upon fluorination of polymeric backbone.[107–109] By the SCLC approach, the hole mobilities of CH_3O-PTAA, CH_3-PTAA, and F-PTAA films were calculated to be 5.59×10^{-5}, $4.38 \times 10^{-5,}$ and 2.2×10^{-5} $cm^2V^{-1}S^{-1}$, respectively.[29,84] The hole mobility of PDTIDTBT was calculated to be 5.24×10^{-4} cm^2 V s^{-1}, as determined by the SCLC method, even higher than spiro-OMeTAD ($8.1\times 10^{-5}cm^2$ V s^{-1}) [44] suggesting its suitability as a dopant-free HTM.[44,110] The high planar ladder-like conjugated backbone of IDTB, as well as S…O intramolecular interactions resulted in high hole mobility and passivation effect for perovskite. The high hole mobility of undoped IDTB (2.89×10^{-5} cm^2 V s^{-1}) was slightly lower than that of doped spiro-OMeTAD (5.97×10^{-5} cm^2 V s^{-1}). [9] The charge-transporting capability in PDTPC film was calculated by SCLC measurement. PDTPC film exhibited hole mobility as high as 3.98×10^{-3} cm^2 V s^{-1}, even higher than that of non-dopant Spiro-OMeTAD (4.71×10^{-4} cm^2 V s^{-1}), which is the result of high planarity, excellent electron-donating capacity, and narrow band gap of DTPC unit of the polymer.[45] The hole mobility ~ 1.90×10^{-3} cm^2 V s^{-1} for PPY2 resulted in strong inter-chain interactions.[46] For RCP copolymer the hole mobility (3.09×10^{-3} cm^2 V s^{-1}) was even higher than that of P-OR (1.85×10^{-3} cm^2 V s^{-1}) and P-R (0.65×10^{-3} cm^2 V s^{-1}) due to more strongly directed face-on orientation.[75] The electron mobility of NDP-V as ETM determined by SCLC as 2.5×10^{-3} cm^2 V s^{-1} comparable to that of $PC_{61}BM$, so it is potentially excellent ETM to replace costly and unstable $PC_{61}BM$.[96],[49] Although the electron mobility of PFN-2TNDI (4.8×10^{-4} cm^2 V s^{-1}) was slightly lower than that of PCBM, it is a competitive polymeric ETM in terms of charge transport characteristics.[51]

The investigation of HOMO and LUMO energy levels is a method to estimate the suitability of polymer as HTM or ETM in PSCs.[43] To find the effect of substituent on

the energy level and the electronic properties of polymeric materials photoelectron spectroscopy in the air (PESA) was measured. The mesomeric electron-donating ability of CH_3O at the *p*-position of CH_3O-PTAA resulted in a slightly higher HOMO energy level (-5.17 eV) compared with that of CH_3-PTAA (-5.20 eV) leading to a higher doping ability and conductance. The introduction of a fluorine atom at the para position instead of a methyl group at F-PTAA lowered the HOMO energy level of the polymer to -5.52 eV due to the dominant inductive effect of the fluorine atom.[29,84] The energy level of HOMO and LUMO could influence by the BTD/HT ratio in the BTD/P3HT copolymer. Through the voltammetry technique, the energy level of HOMO was detected in BTD/P3HT and it was found the presence of BTD moieties shifted the HOMO level from – 5.00 eV in commercial P3HT to -5.14 eV in BTD/P3HT.[43] For PDTIDTBT, HOMO and LUMO energy levels of -5.35 and -3.29 eV (with a band gap of 2.06 eV) were obtained from CV measurements.[44] The HOMO energy level of IDTB was estimated to be -5.20 eV with an optical bandgap of 2.19 eV by photoelectron spectroscopy. This energy level was even lower than that of Spiro-OMeTAD (-5.12 eV) which allows for achieving a higher V_{oc} value of the device.[9] In a D-A copolymer like PDTPC, the donor units increase the HOMO energy level due to extended conjugation length and the acceptor ones decrease the HOMO level. The HOMO level of -5.11 eV with an optical bandgap of 1.60 eV for PDTPC was measured by CV.[45] Accordingly, the PPY2 has an aligned HOMO energy level (-5.17 eV from CV and UPS) with a perovskite layer.[46] CV was used to determine the electrochemical characteristics of PFN-2TNDI. The study of frontier molecular orbitals demonstrated that the LUMO (-3.84 eV) and HOMO (-5.57 eV) level of this copolymer was slightly lower than the conduction band (CB) and the valance band (VB) of perovskite film, respectively. The suitable hole blocking property makes it a promising candidate for ETM.[51] RCP copolymer including P-OR and P-R showed [75] a HOMO energy level of -5.51 eV, slightly deeper than that of the perovskite layer ($CH_3NH_3PbI_3$; -5.43 eV). PNVT-8, N2200, (PNDI2OD)TT showed the LUMO level of ~ -3.90 eV and HOMO levels from -5.61 eV ~ -5.82 eV which were compatible with the energy levels of perovskite and also similar to the LUMO/HOMO levels of PCBM, making them as valuable ETM candidate[50,99] (**Fig. 10**).[50] It seems the presence of vinyl linkages in PNVT-8 caused a higher energy level of HOMO as compared with N2200 and (PNDI2OD)TT while having a negligible effect on their LUMO energy level.[99] One of the deeper LUMO

levels among NDI-based polymers belongs to P(NDI2DT-TTCN) with a LUMO level of -4.14 eV which suggests its suitability as an electron-transport layer.[52]

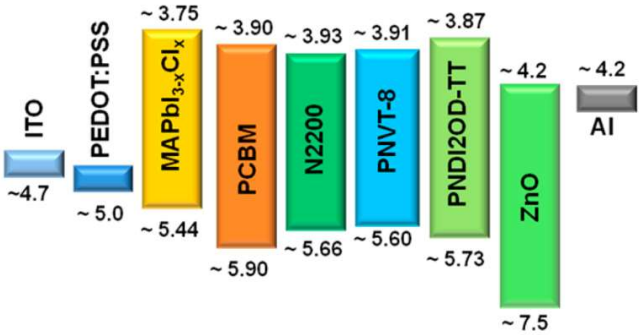

Fig. 10. Energy level alignment used in the device.[50] Copyright 2015, American Chemical Society.

Conclusions and Outlook

The use of rational polymer is one of the decisive means to improve the reliability of perovskite solar cells such as stability and performance enhancement. We scrutinized and summarized the recent progress in the use of polymers for improving the stability and photovoltaics parameters when employed as hole transporting material (HTM), electron transporting material (ETM), interfacial layer, and additives into the perovskite, or HTM, and ETM. We quantify the use of effective and facile polymers along with their synthetic ways for perovskite solar cells and detailed their merits and shortcomings. An array of detailed characterization techniques of polymer using NMR, FTIR spectroscopy, molecular weight analyses, thermal stability, and optical and electrochemical properties are probed to unravel the underlying hypothesis of its use. Polymers have an enormous potential to contribute to the success of perovskite solar cell commercialization and a window of opportunity exists to improve lifetime, photovoltaic performances, and cost reduction through its use.

Conflicts of interest

There are no known conflicts to declare.

Acknowledgements

This work received funding from the European Union H2020 Programme under a European Research Council Consolidator grant [MOLEMAT, 726360] and from the Spanish Ministry of Science and Innovation (PID2020-117855RB-I00) and ELKARTEK (ENSOL2).

Notes and references

Abbreviations: a-Si, amorphous silicon; BDT, benzo[1,2-b:4,5:b']dithiophene; BP, black phosphorus; BT, 2,1,3-benzothiadiazole; CdTe, cadmium telluride; CTM, charge transporting material; CIGS, copper indium gallium selenide; CIS, copper indium selenide; CNT, carbon nanotube; c-Si, crystalline silicon; D-A, donor-acceptor; DI, dimethyl itaconate; DSSC, dye-sensitized solar cell; DTPS, dithienopiceno carbazole; E2CA, ethyl 2-cyanoacrylate; ETM, electron transporting material; $FAPbI_3$, formamidinium lead iodide; FF, fill factor; F8TBT, poly[(9,9-dioctyluorene)-2,7-diylalt-(4,7-bis(3-hexylthien-5-yl)2,1,3-benzothiadiazole)-2',2"-diyl]; FTO, fluorine-doped tin oxide; $Ga(acac)_3$, gallium(iii) acetylacetonate; (HT), 3-hexylthiophene; HTM, hole transporting material; IDTB copolymer, poly(1,4-(2,5-bis((2-butyloctyloxyphenylene)-2,7-(5,5,10,10-tetrakis(4-hexylphenyl)-5,10-dihydro-s-indaceno[2,1-b:6,5-b']dithiophene)); J_{sc}, short-circuit current density; N2200, poly {{N,N´-bis(2-octyldodecyl)-1,4,5,8-naphthalene diimide-2,6-diyl]-alt-5,5´-(2,2´-bithiophene)};nc-Si, nanocrystalline silicon; NDI, naphthalene diimide; NDP-V, poly(naphthodiperylenetetraimide-vinylene); OPV, organic photovoltaic; PDI, perylene diimide; PAGG, polymerization-assisted grain growth; PANI, polyaniline; PASP, poly aspartic acid sodium; PCBM, [6,6]-phenyl-C61-butyric acid methyl ester;$PC_{61}BM$, [6,6]-phenyl-C61-butyric acid methyl ester; PCE, power conversion efficiency; PDTIDTBT, poly{2,7-[(5,5-bis(3',7'-dimethyloctyl)-5H-1,8-dithia-as-indacenone]-alt-5,5-[5',6'-bis(octyloxy)-4',7'-di-2-thienyl-2',1',3'-benzothiadia-zole]}; PEDOT:PSS, poly(3,4-ethylenedioxythiophene):poly(styrenesulfonate); PEG, polyethylene glycol; PEIE, poly(ethylenimine) ethoxylated; PEO, polyethylene oxide; PEOXA, poly(2-ethyl-2-oxazoline); PFN-I, poly[(9,9-bis(3-((*N,N*-dimethyl)-*N*-ethyl-ammonium)-propyl)-2,7-fluorene)-alt-2,7-(9,9-dioctylfluorene)]di-iodide; P3HT, poly(3-hexylthiophene); PMMA, poly(methyl methacrylate); P(NDI2OD-T2), poly {{N,N´-bis(2-octyldodecyl)-1,4,5,8-naphthalene diimide-2,6-diyl]-alt-5,5´-(2,2´-bithiophene)}; PNVT-8, poly {{N,N´-bis(alkyl)-1,4,5,8-naphthalene diimide-2,6-diyl]-alt-5,5´-di(thiophene-2-yl)-2,2´-(E)-2-(2-(thiophen-2-yl)vinyl)thiophene]}; polyTPD, poly(*N,N'*-bis(4-butylphenyl)-*N,N'*-bis(phenyl)benzidine); PPY, pyridine-based polymer; PS, polystyrene; PSC, perovskite solar cell; PSK, perovskite; PTAA, poly-[bis(4-phenyl)(2,4,6-trimethylphenyl)amine]; P3TMAHT, poly[3-(6-trimethylammoniumhexyl)thiophene]; PTQ10, poly[(thiophene)-alt-(6,7-difluoro-2-(2-hexyldecyloxy)quinoxaline)]; PV, photovoltaic; PVDF-TrFE, polyvinylidene-trifluoroethylene copolymer; PVP, poly(vinylpyrrolidone); QDSSC, quantum dot sensitized solar cell; RCP, random copolymer; RH, relative humidity; spiro-OMeTAD, 2,2´,7,7´-tetrakis-(N,N-di-p-methoxyphenylamine)9,9´-spirobifluorene; SPM, SnO_2-in-polymer matrix; SWNT, single walled nanotube; TAPC, 4,4'-cyclohexylidenebis[*N,N*-bis(4-methyl-phenyl) benzenamine]; TS-MPc, metal-phthalocyanine−tetrasulfonated acid tetrasodium salt ; V_{oc}, open-circuit voltage; $(ZnP)_n$, polymeric zinc porphyrin.

References:

1 K. Choi, H. Choi, J. Min, T. Kim, D. Kim, S. Y. Son, G.-W. Kim, J. Choi and T. Park, *Sol. RRL*, 2020, **4**, 1900251.

2 W. Hou, Y. Xiao, G. Han and J.-Y. Lin, *Polymers (Basel).*, 2019, **11**, 143.

3 S. R. Fatemi Shariat Panahi, A. Abbasi, V. Ghods and M. Amirahmadi, *J. Mater. Sci. Mater. Electron.*, 2020, **31**, 11527–11537.

4 S. Ananthakumar, J. R. Kumar and S. M. Babu, 2019, pp. 305–339.

5 Y. Hamakawa, Ed., *Thin-Film Solar Cells*, Springer Berlin Heidelberg, Berlin, Heidelberg, 2004, vol. 13.

6 O. K. Simya, P. Radhakrishnan, A. Ashok, K. Kavitha and R. Althaf, *Handb. Nanomater. Ind. Appl.*, 2018, 751–767.

7 J. Kettle, M. Aghaei, S. Ahmad, A. Fairbrother, S. Irvine, J. Jacobsson, S. Kazim, V. Kazukauskas, D. Lamb, K. Lobato, G. Mousdis, G. Oreski, A. Reinders, J. Schmitz, P. Yilmaz, M. Theelen.*Prog Photovolt Res Appl*. 2022

8 B. Li, K. Yang, Q. Liao, Y. Wang, M. Su, Y. Li, Y. Shi, X. Feng, J. Huang, H. Sun and X. Guo, *Adv. Funct. Mater.*, 2021, **31**, 2100332.

9 T. Chawanpunyawat, P. Funchien, P. Wongkaew, N. Henjongchom, A. Ariyarit, S. Ittisanronnachai, S. Namuangruk, R. Cheacharoen, T. Sudyoadsuk, F. Goubard and V. Promarak, *ChemSusChem*, 2020, **13**, 5058–5066.

10 L. Calió, S. Kazim, M. Grätzel and S. Ahmad, *Angew. Chemie Int. Ed.*, 2016, **55**, 14522–14545.

11 H. J. Snaith, *Nat. Mater.*, 2018, **17**, 372–376.

12 M. A. Green, A. Ho-Baillie and H. J. Snaith, *Nat. Photonics*, 2014, **8**, 506–514.

13 P. P. Boix, S. Agarwala, T. M. Koh, N. Mathews and S. G. Mhaisalkar, *J. Phys. Chem. Lett.*, 2015, **6**, 898–907.

14 A. Kojima, K. Teshima, Y. Shirai and T. Miyasaka, *J. Am. Chem. Soc.*, 2009, **131**, 6050–6051.

15 X. Liu, Y. Cheng, C. Liu, T. Zhang, N. Zhang, S. Zhang, J. Chen, Q. Xu, J. Ouyang and H. Gong, *Energy Environ. Sci.*, 2019, **12**, 1622–1633.
16 Y. Wu, D. Wang, J. Liu and H. Cai, *Nanomaterials*, 2021, **11**, 775.
17 T. Ji, Y.-K. Wang, L. Feng, G.-H. Li, W.-Y. Wang, Z.-F. Li, Y.-Y. Hao and Y.-X. Cui, *Rare Met.*, 2021, **40**, 2690–2711.
18 A. Marchioro, J. Teuscher, D. Friedrich, M. Kunst, R. van de Krol, T. Moehl, M. Grätzel and J.-E. Moser, *Nat. Photonics*, 2014, **8**, 250–255.
19 W. Chen, Y. Zhu, J. Xiu, G. Chen, H. Liang, S. Liu, H. Xue, E. Birgersson, J. W. Ho, X. Qin, J. Lin, R. Ma, T. Liu, Y. He, A. M.-C. Ng, X. Guo, Z. He, H. Yan, A. B. Djurišić and Y. Hou, *Nat. Energy*, , DOI:10.1038/s41560-021-00966-8.
20 Z. Yao, F. Zhang, L. He, X. Bi, Y. Guo, Y. Guo, L. Wang, X. Wan, Y. Chen and L. Sun, *Angew. Chemie Int. Ed.*, , DOI:10.1002/anie.202201847.
21 D. Wang, T. Ye and Y. Zhang, *J. Mater. Chem. A*, 2020, **8**, 20819–20848.
22 L. Wan, W. Zhang, Y. Wu, X. Li, C. Song, Y. He, W. Zhang and J. Fang, *Nanoscale*, 2019, **11**, 9281–9286.
23 Q. Dong, Z. Wang, K. Zhang, H. Yu, P. Huang, X. Liu, Y. Zhou, N. Chen and B. Song, *Nanoscale*, 2016, **8**, 5552–5558.
24 D. Bi, C. Yi, J. Luo, J.-D. Décoppet, F. Zhang, S. M. Zakeeruddin, X. Li, A. Hagfeldt and M. Grätzel, *Nat. Energy*, 2016, **1**, 16142.
25 D. I. Kim, J. W. Lee, R. H. Jeong and J.-H. Boo, *Sci. Rep.*, 2022, **12**, 697.
26 S. Wang, Z. Zhang, Z. Tang, C. Su, W. Huang, Y. Li and G. Xing, *Nano Energy*, 2021, **82**, 105712.
27 J. H. Heo, S. H. Im, J. H. Noh, T. N. Mandal, C.-S. Lim, J. A. Chang, Y. H. Lee, H. Kim, A. Sarkar, M. K. Nazeeruddin, M. Grätzel and S. Il Seok, *Nat. Photonics*, 2013, **7**, 486–491.
28 W. S. Yang, J. H. Noh, N. J. Jeon, Y. C. Kim, S. Ryu, J. Seo and S. Il Seok, *Science (80-.).*, 2015, **348**, 1234–1237.
29 Y. Kim, G. Kim, N. J. Jeon, C. Lim, J. Seo and B. J. Kim, *ACS Energy Lett.*, 2020, **5**, 3304–3313.
30 M. M. Tepliakova, A. V. Akkuratov, S. A. Tsarev and P. A. Troshin, *Tetrahedron Lett.*, 2020, **61**, 152317.
31 C. Y. Xu, W. Hu, G. Wang, L. Niu, A. M. Elseman, L. Liao, Y. Yao, G. Xu, L. Luo, D. Liu, G. Zhou, P. Li and Q. Song, *ACS Nano*, 2020, **14**, 196–203.
32 W. Dong, S. Xiong, J. Yang, W. Qiao, Q. Zeng, X. Wang, Y. Yao and Q. Bao, *Org. Electron.*, 2021, **89**, 106052.
33 X. Zheng, Y. Hou, C. Bao, J. Yin, F. Yuan, Z. Huang, K. Song, J. Liu, J. Troughton, N. Gasparini, C. Zhou, Y. Lin, D.-J. Xue, B. Chen, A. K. Johnston, N. Wei, M. N. Hedhili, M. Wei, A. Y. Alsalloum, P. Maity, B. Turedi, C. Yang, D. Baran, T. D. Anthopoulos, Y. Han, Z.-H. Lu, O. F. Mohammed, F. Gao, E. H. Sargent and O. M. Bakr, *Nat. Energy*, 2020, **5**, 131–140.
34 Y. Xia and S. Dai, *J. Mater. Sci. Mater. Electron.*, 2021, **32**, 12746–12757.
35 J.-Y. Jeng, Y.-F. Chiang, M.-H. Lee, S.-R. Peng, T.-F. Guo, P. Chen and T.-C. Wen, *Adv. Mater.*, 2013, **25**, 3727–3732.
36 L. Hu, M. Li, K. Yang, Z. Xiong, B. Yang, M. Wang, X. Tang, Z. Zang, X. Liu, B. Li, Z. Xiao, S. Lu, H. Gong, J. Ouyang and K. Sun, *J. Mater. Chem. A*, 2018, **6**, 16583–16589.
37 E. Edri, S. Kirmayer, D. Cahen and G. Hodes, *J. Phys. Chem. Lett.*, 2013, **4**, 897–902.
38 E. H. Jung, N. J. Jeon, E. Y. Park, C. S. Moon, T. J. Shin, T.-Y. Yang, J. H. Noh and J. Seo, *Nature*, 2019, **567**, 511–515.
39 N. Yaghoobi Nia, E. Lamanna, M. Zendehdel, A. L. Palma, F. Zurlo, L. A. Castriotta

and A. Di Carlo, *Small*, 2019, **15**, 1904399.
40 M. J. Jeong, K. M. Yeom, S. J. Kim, E. H. Jung and J. H. Noh, *Energy Environ. Sci.*, 2021, **14**, 2419–2428.
41 L. M. Kozycz, D. Gao and D. S. Seferos, *Macromolecules*, 2013, **46**, 613–621.
42 B. Burkhart, P. P. Khlyabich and B. C. Thompson, *ACS Macro Lett.*, 2012, **1**, 660–666.
43 F. De Rossi, G. Renno, B. Taheri, N. Yaghoobi Nia, V. Ilieva, A. Fin, A. Di Carlo, M. Bonomo, C. Barolo and F. Brunetti, *J. Power Sources*, 2021, **494**, 229735.
44 M. M. Tavakoli, R. Po, G. Bianchi, C. Carbonera and J. Kong, *Sol. RRL*, 2021, **5**, 2000801.
45 Z. Zhang, L. Liang, L. Deng, L. Ren, N. Zhao, J. Huang, Y. Yu and P. Gao, *ACS Appl. Mater. Interfaces*, 2021, **13**, 6688–6698.
46 X. Sun, Z. Li, X. Yu, X. Wu, C. Zhong, D. Liu, D. Lei, A. K. -Y. Jen, Z. Li and Z. Zhu, *Angew. Chemie Int. Ed.*, 2021, **60**, 7227–7233.
47 C. Liu, J. Sun, X.-F. Jiang, L. Huang, Q. Lou, Y.-B. Cheng, S. Song and Z. Ge, *Sci. China Chem.*, 2021, **64**, 281–292.
48 Q. Jiang, X. Zhang and J. You, *Small*, 2018, **14**, 1801154.
49 K. Jiang, F. Wu, L. Zhu and H. Yan, *ACS Appl. Mater. Interfaces*, 2018, **10**, 36549–36555.
50 W. Wang, J. Yuan, G. Shi, X. Zhu, S. Shi, Z. Liu, L. Han, H.-Q. Wang and W. Ma, *ACS Appl. Mater. Interfaces*, 2015, **7**, 3994–3999.
51 C. Sun, Z. Wu, H.-L. Yip, H. Zhang, X.-F. Jiang, Q. Xue, Z. Hu, Z. Hu, Y. Shen, M. Wang, F. Huang and Y. Cao, *Adv. Energy Mater.*, 2016, **6**, 1501534.
52 H. Il Kim, M.-J. Kim, K. Choi, C. Lim, Y.-H. Kim, S.-K. Kwon and T. Park, *Adv. Energy Mater.*, 2018, **8**, 1702872.
53 Q. Wang, Q. Dong, T. Li, A. Gruverman and J. Huang, *Adv. Mater.*, 2016, **28**, 6734–6739.
54 O. Malinkiewicz, A. Yella, Y. H. Lee, G. M. Espallargas, M. Graetzel, M. K. Nazeeruddin and H. J. Bolink, *Nat. Photonics*, 2014, **8**, 128–132.
55 L. Meng, C. Sun, R. Wang, W. Huang, Z. Zhao, P. Sun, T. Huang, J. Xue, J.-W. Lee, C. Zhu, Y. Huang, Y. Li and Y. Yang, *J. Am. Chem. Soc.*, 2018, **140**, 17255–17262.
56 E. Akman and S. Akin, *Adv. Mater.*, 2021, **33**, 2006087.
57 X. Lian, J. Chen, S. Shan, G. Wu and H. Chen, *ACS Appl. Mater. Interfaces*, 2020, **12**, 46340–46347.
58 J. Wu, Y. Cui, B. Yu, K. Liu, Y. Li, H. Li, J. Shi, H. Wu, Y. Luo, D. Li and Q. Meng, *Adv. Funct. Mater.*, 2019, **29**, 1905336.
59 B. Li, Y. Xiang, K. D. G. I. Jayawardena, D. Luo, J. F. Watts, S. Hinder, H. Li, V. Ferguson, H. Luo, R. Zhu, S. R. P. Silva and W. Zhang, *Sol. RRL*, 2020, **4**, 2000060.
60 H. Zhang, H. Azimi, Y. Hou, T. Ameri, T. Przybilla, E. Spiecker, M. Kraft, U. Scherf and C. J. Brabec, *Chem. Mater.*, 2014, **26**, 5190–5193.
61 Q. Xue, Z. Hu, J. Liu, J. Lin, C. Sun, Z. Chen, C. Duan, J. Wang, C. Liao, W. M. Lau, F. Huang, H.-L. Yip and Y. Cao, *J. Mater. Chem. A*, 2014, **2**, 19598–19603.
62 P. Zhou, Z. Fang, W. Zhou, Q. Qiao, M. Wang, T. Chen and S. Yang, *ACS Appl. Mater. Interfaces*, 2017, **9**, 32957–32964.
63 M. Sun, H. Zhang, C. Liang, C. Ji, X. Jing, F. Sun, Q. Song, F. You and Z. He, *Adv. Mater. Interfaces*, 2020, **7**, 2000412.
64 Q. Xue, Z. Hu, C. Sun, Z. Chen, F. Huang, H.-L. Yip and Y. Cao, *RSC Adv.*, 2015, **5**, 775–783.
65 C.-Y. Chang, C.-Y. Chu, Y.-C. Huang, C.-W. Huang, S.-Y. Chang, C.-A. Chen, C.-Y. Chao and W.-F. Su, *ACS Appl. Mater. Interfaces*, 2015, **7**, 4955–4961.
66 Y. Zhao, P. Zhu, M. Wang, S. Huang, Z. Zhao, S. Tan, T. Han, J. Lee, T. Huang, R.

Wang, J. Xue, D. Meng, Y. Huang, J. Marian, J. Zhu and Y. Yang, *Adv. Mater.*, 2020, **32**, 1907769.
67 Y. Bai, H. Yu, Z. Zhu, K. Jiang, T. Zhang, N. Zhao, S. Yang and H. Yan, *J. Mater. Chem. A*, 2015, **3**, 9098–9102.
68 J. Wei, F. Guo, X. Wang, K. Xu, M. Lei, Y. Liang, Y. Zhao and D. Xu, *Adv. Mater.*, 2018, **30**, 1805153.
69 S. N. Habisreutinger, T. Leijtens, G. E. Eperon, S. D. Stranks, R. J. Nicholas and H. J. Snaith, *Nano Lett.*, 2014, **14**, 5561–5568.
70 W. Li, C. Liu, Y. Li, W. Kong, X. Wang, H. Chen, B. Xu and C. Cheng, *Sol. RRL*, 2018, **2**, 1800173.
71 S. H. Lee, S. Hong, H. H. Lee and H. J. Kim, *Adv. Mater. Interfaces*, 2021, **8**, 2001891.
72 Q. Wang and A. Abate, *Adv. Mater. Interfaces*, 2018, **5**, 1800264.
73 Y. Zhao, J. Wei, H. Li, Y. Yan, W. Zhou, D. Yu and Q. Zhao, *Nat. Commun.*, 2016, **7**, 10228.
74 J. Kim, S. Kim, C. Zuo, M. Gao, D. Vak and D. Kim, *Adv. Funct. Mater.*, 2019, **29**, 1809194.
75 G.-W. Kim, G. Kang, J. Kim, G.-Y. Lee, H. Il Kim, L. Pyeon, J. Lee and T. Park, *Energy Environ. Sci.*, 2016, **9**, 2326–2333.
76 J. Xiong, Y. Qi, Q. Zhang, D. Box, K. Williams, J. Tatum, P. Das, N. R. Pradhan and Q. Dai, *ACS Appl. Energy Mater.*, 2021, **4**, 1815–1823.
77 H. Usta, A. Facchetti and T. J. Marks, *Acc. Chem. Res.*, 2011, **44**, 501–510.
78 A. A. El-Shehawy, N. I. Abdo, A. A. El-Barbary and J.-S. Lee, *European J. Org. Chem.*, 2011, **2011**, 4841–4852.
79 H. Zheng, X. Xu, S. Xu, G. Liu, S. Chen, X. Zhang, T. Chen and X. Pan, *J. Mater. Chem. C*, , DOI:10.1039/C8TC05975F.
80 H. Liang, W. D. Wang, S. Mai, X. Lv, J. Fang and J. Cao, *Chem. Eng. J.*, 2022, **429**, 132405.
81 X. Li, W. Zhang, W. Zhang, H.-Q. Wang and J. Fang, *Nano Energy*, 2019, **58**, 825–833.
82 J. Peng, Y. Wu, W. Ye, D. A. Jacobs, H. Shen, X. Fu, Y. Wan, T. Duong, N. Wu, C. Barugkin, H. T. Nguyen, D. Zhong, J. Li, T. Lu, Y. Liu, M. N. Lockrey, K. J. Weber, K. R. Catchpole and T. P. White, *Energy Environ. Sci.*, 2017, **10**, 1792–1800.
83 J. Peng, J. I. Khan, W. Liu, E. Ugur, T. Duong, Y. Wu, H. Shen, K. Wang, H. Dang, E. Aydin, X. Yang, Y. Wan, K. J. Weber, K. R. Catchpole, F. Laquai, S. Wolf and T. P. White, *Adv. Energy Mater.*, 2018, **8**, 1801208.
84 Y. Kim, E. H. Jung, G. Kim, D. Kim, B. J. Kim and J. Seo, *Adv. Energy Mater.*, 2018, **8**, 1801668.
85 M. Wang, H. Wang, W. Li, X. Hu, K. Sun and Z. Zang, *J. Mater. Chem. A*, 2019, **7**, 26421–26428.
86 H. M. Alishah, F. P. G. Choi, F. Kuruoglu, A. Erol and S. Gunes, *Electrochim. Acta*, 2021, **388**, 138658.
87 B. Wang, F. Wu, S. Bi, J. Zhou, J. Wang, X. Leng, D. Zhang, R. Meng, B. Xue, C. Zong, L. Zhu, Y. Zhang and H. Zhou, *J. Mater. Chem. A*, 2019, **7**, 23895–23903.
88 D. Yang, X. Zhang, K. Wang, C. Wu, R. Yang, Y. Hou, Y. Jiang, S. Liu and S. Priya, *Nano Lett.*, 2019, **19**, 3313–3320.
89 T. Yamamoto, S.-B. Kim and T. Koizumi, *Polym. J.*, 2009, **41**, 810–815.
90 R. D. McCullough and R. D. Lowe, *J. Chem. Soc. Chem. Commun.*, 1992, 70.
91 R. D. McCullough, S. Tristram-Nagle, S. P. Williams, R. D. Lowe and M. Jayaraman, *J. Am. Chem. Soc.*, 1993, **115**, 4910–4911.
92 R. D. McCullough, R. D. Lowe, M. Jayaraman and D. L. Anderson, *J. Org. Chem.*, 1993, **58**, 904–912.

93 A. Kiriy, V. Senkovskyy and M. Sommer, *Macromol. Rapid Commun.*, 2011, **32**, 1503–1517.
94 M. Trznadel, A. Pron, M. Zagorska, R. Chrzaszcz and J. Pielichowski, *Macromolecules*, 1998, **31**, 5051–5058.
95 M. M. Tavakoli, R. Po, G. Bianchi, A. Cominetti, C. Carbonera, N. Camaioni, F. Tinti and J. Kong, *Proc. Natl. Acad. Sci.*, 2019, **116**, 22037–22043.
96 Y. Guo, Y. Li, O. Awartani, H. Han, J. Zhao, H. Ade, H. Yan and D. Zhao, *Adv. Mater.*, 2017, **29**, 1700309.
97 Y. Zhong, B. Kumar, S. Oh, M. T. Trinh, Y. Wu, K. Elbert, P. Li, X. Zhu, S. Xiao, F. Ng, M. L. Steigerwald and C. Nuckolls, *J. Am. Chem. Soc.*, 2014, **136**, 8122–8130.
98 A. Luzio, D. Fazzi, D. Natali, E. Giussani, K.-J. Baeg, Z. Chen, Y.-Y. Noh, A. Facchetti and M. Caironi, *Adv. Funct. Mater.*, 2014, **24**, 1151–1162.
99 H. Chen, Y. Guo, Z. Mao, G. Yu, J. Huang, Y. Zhao and Y. Liu, *Chem. Mater.*, 2013, **25**, 3589–3596.
100 D. Fazzi, M. Caironi and C. Castiglioni., *J. Am. Chem. Soc.*, 2011, **133**, 19056–19059.
101 H. Yan, Z. Chen, Y. Zheng, C. Newman, J. R. Quinn, F. Dötz, M. Kastler and A. Facchetti, *Nature*, 2009, **457**, 679–686.
102 T.-A. Chen, X. Wu and R. D. Rieke, *J. Am. Chem. Soc.*, 1995, **117**, 233–244.
103 D. L. Pavia, G. M. Lampman, G. S. Kriz and J. R. Vyvyan, *Introduction to Spectroscopy*, Cengage Learning, 5th edn., 2014.
104 P. Quagliotto and A. Fin, *Lett. Org. Chem.*, 2018, **15**, 991–1006.
105 F. Zhang, Z. Yao, Y. Guo, Y. Li, J. Bergstrand, C. J. Brett, B. Cai, A. Hajian, Y. Guo, X. Yang, J. M. Gardner, J. Widengren, S. V. Roth, L. Kloo and L. Sun, *J. Am. Chem. Soc.*, 2019, **141**, 19700–19707.
106 Z. Yao, F. Zhang, Y. Guo, H. Wu, L. He, Z. Liu, B. Cai, Y. Guo, C. J. Brett, Y. Li, C. V. Srambickal, X. Yang, G. Chen, J. Widengren, D. Liu, J. M. Gardner, L. Kloo and L. Sun, *J. Am. Chem. Soc.*, 2020, **142**, 17681–17692.
107 Z. Li, J. Lu, S.-C. Tse, J. Zhou, X. Du, Y. Tao and J. Ding, *J. Mater. Chem.*, 2011, **21**, 3226.
108 T. L. Nguyen, H. Choi, S.-J. Ko, M. A. Uddin, B. Walker, S. Yum, J.-E. Jeong, M. H. Yun, T. J. Shin, S. Hwang, J. Y. Kim and H. Y. Woo, *Energy Environ. Sci.*, 2014, **7**, 3040–3051.
109 W. Zhang, J. Smith, R. Hamilton, M. Heeney, J. Kirkpatrick, K. Song, S. E. Watkins, T. Anthopoulos and I. McCulloch, *J. Am. Chem. Soc.*, 2009, **131**, 10814–10815.
110 B. Xu, D. Bi, Y. Hua, P. Liu, M. Cheng, M. Grätzel, L. Kloo, A. Hagfeldt and L. Sun, *Energy Environ. Sci.*, 2016, **9**, 873–877.